Synthesis and adsorption characteristics of grafted hydrazinyl amine magnetite-chitosan for Ni(II) and Pb(II) recovery

Mohammed F. Hamza, Yuezhou Wei, H. I. Mira, Hala Abdul Rahman, Eric Guibal

Synthesis and adsorption characteristics of grafted hydrazinyl amine magnetite-chitosan for Ni(II) and Pb(II) recovery

Mohammed F. HAMZA,[(a-c)] Yuezhou WEI,[(a)] H. I. MIRA, [(c)] Adel A.-H. Abdel-Rahman,[(d)] Eric GUIBAL[(b)]

(a) School of Resources, Environment and Materials, Guangxi University, 100 Daxue Road, Nanning 530004, China
(b) C2MA, IMT – Mines Ales, Univ. Montpellier, Alès, France
(c) Nuclear Materials Authority, POB 530, El-Maadi, Cairo, Egypt (d) Faculty of Science, Menoufia University (Egypt)

Correspondence:
Eric Guibal, Ph: +33 (0)466782734; Email: Eric.Guibal@mines-ales.fr
Mohammed F. Hamza, Email: m_fouda21@hotmail.com

Emails: hamedmira@yahoo.com (H.I.M.); yzwei@gxu.edu.cn (Y.W.); adelnassar63@yahoo.com (A.A-H.A-R)

Abstract:

The sorption properties of a functionalized magnetic chitosan sorbent have been investigated for the recovery of Ni(II) and Pb(II) from aqueous solutions. This material was prepared by one-pot co-precipitation of chitosan with formation of magnetic core, followed by a series of grafting step to immobilize hydrazinyl amine derivative at the surface of chitosan layer. The physico-chemical characteristics of this composite material were investigated using FTIR, XRD, thermogravimetric, titration, elemental analyses. In a second step, the sorbent was tested for heavy metal sorption on synthetic solutions through the study of pH effect, sorption isotherms and uptake kinetics, selective sorption (in function of pH), metal desorption and sorbent recycling. Sorption isotherms were modeled using the Sips equation while the uptake kinetics was fitted by the pseudo-second order rate equation. The sorption capacity reached 4.3 mmol Ni g^{-1} and 2.5 mmol Pb g^{-1} but the sorbent was more selective to Pb(II) over Ni(II), especially in acidic conditions. The decrease in sorption capacity at the fifth cycle does not exceed 8 %. In the final step of the study, the sorbents were successfully applied for metal recovery from multi-metal synthetic solution and from a contaminated stormwater collected in a local mining area.

Keywords: chitosan derivative; sorption isotherms; uptake kinetics; sorbent recycling; nickel; lead; wastewater treatment.

1. Introduction

The mining activity is generating direct (effluents from ore processing) and indirect contamination of soils and water bodies in large surrounding area due to metal mobility via leaching (by infiltration of rain water through mine tailing), flying dust, etc. The potential impact of metal ions on human health and biotope communities has driven strong reinforcement of national and international regulations concerning wastewater discharge into the environment. The necessity to recycle water streams is also of critical importance in many countries, due to increasing demand and limited resources. The removal of toxic metals is thus a challenge for Nature protection but also, in many cases, the study of the impact on impact should be measured before authorizing implantation of new industrial activities. The recovery of valuable resources, such as critical or strategic metals, is also contributing to justify active studies and applications of hydrometallurgy in a world requesting greener production, improving circular economy. Metal recovery is thus a critical topic that motivated strong developments for the last decades through manufacturing new materials and designing new processes.

Depending on the composition of these effluents, including pH, metal concentrations, presence of competitor ions, etc., different methods can be applied. For high metal concentrations (such as leachates produced during ore treatment) the most competitive processes consist of precipitation [1, 2] and solvent extraction [3-5]. However, they are weakly selective (for precipitation) or expensive with potential environmental impact (extractant and solvent loss for solvent extraction processes) when the concentration of valuable metals decreases. Alternative processes are thus more appropriate for dilute effluents. Sorption processes are generally preferred when metal concentration does not exceed 100-150 mg L^{-1}. At higher concentrations the expected concentrating effect of sorption/desorption may be too low to be competitive against other processes such as solvent

extraction (especially for valuable metals) or precipitation (for hazardous metals). Many ion-exchange and chelating resins have been designed for hydrometallurgy and analytical applications [6-9]. Alternatively solvent impregnated resins can be used for metal recovery combining the high stability of porous synthetic resin and the extraction properties of solvent extractants [10, 11]. The major criteria used for designing resins consist of high density of reactive groups (coupled with hydrophilic behavior), good diffusion properties (for fast kinetics associated to the small size of particles and high porosity of polymer or inorganic support), and fine hydrodynamic properties (for applications in fixed-bed columns: shape size homogeneity, etc.). Despite the strong development of resin industry, there is still a need to develop more competitive materials for the treatment of much diluted effluents. This challenge may explain the intense research carried out for the last decades on the development of biosorption processes [12-14]. These materials issued from agriculture [15] or fisheries [16] by-products make profit of surface reactive groups that are similar to those present on synthetic resins; obtained from renewable resources they can be considered, in some cases, as a valorization of waste products.

Chitosan is an emblematic example of biosorbents that retained a great attention for metal sorption since the 70's [17-20]. This aminopolysaccharide is obtained by deacetylation of chitin (present in the exoskeleton of arthropods and the cell wall of fungi). The biopolymer being soluble in most acid solutions (except sulfuric acid media) must be cross-linked for increasing its chemical stability in a wide range of pH values. The presence of primary amine groups may explain its strong affinity for cation binding in near neutral pH, while the protonation of amine functions brings the possibility to bind metal anions in acidic solutions. One of the main drawbacks of chitosan is the poor porosity of the polymer that induces slow mass transfer properties and slow kinetics. This drawback can be overcome by: (a) conditioning the biopolymer under the form of hydrogel beads (decrease in crystallinity and

expansion of the polymer network) providing the control of drying conditions (or the use of wet hydrogel) [21], (b) decreasing the size of the sorbent particles (at the expense of difficulties in solid/liquid separation, or head loss when used in fixed-bed columns). Small particles can be also used while preparing composite magnetic chitosan particles [22]. This method allows a simple solid/liquid phase separation at the end of the sorption process, in addition to the fast transfer properties associated to the thin polymer coating layer deposited at the surface of magnetite particles.

The magnetic chitosan particles can be obtained by coating the biopolymer on magnetite micro- or nano-particles or alternatively by simultaneous co-precipitation of chitosan and in situ production of magnetite particles (by pH-controlled hydrothermal precipitation of iron(II) and iron(III) precursors). This is this one-pot synthesis procedure that was selected for preparing the composite magnetic chitosan material used in the present work [23]. In order to improve sorption properties many different reactive groups have been used for decorating the biopolymer including EDTA and analogues [24], amino-acids [25], amidoxime [26, 27], aminophosphonate [28], sulfur compound [29], etc. In a previous work a magnetic sorbent was prepared by functionalization of chitosan magnetic particles [30]: a hydrazide derivative was immobilized on glycine-ester functionalities and the sorbent was successfully tested for the sorption of uranyl, copper and zinc ions from synthetic pure or binary solutions; the present work use this sorbent for investigating the recovery of Ni(II) and Pb(II) before testing the treatment of synthetic complex solution and real contaminated effluent.

2. Materials & Methods

2.1. Materials & synthesis of sorbent

Nickel chloride, lead chloride (source for Ni(II), and Pb(II) respectively) were obtained from Sigma-Aldrich. Stock metal solutions were prepared by salt dissolving in Milli-Q water at the

concentration of 1 g L^{-1}. Chitosan (deacetylation degree: 90.5 %) was supplied by Sigma-Aldrich (Taufkirchen, Germany). The biopolymer was used as received, without purification. Absolute ethanol and epichlorohydrin were obtained from Fluka AG (Switzerland). Other reagents were supplied by Prolabo (VWR, France).

2.2. Synthesis procedure

(a) Preparation of magnetic chitosan micro-particles (MG-CH)

The magnetite was prepared by the hydrothermal co-precipitation method, the so-called Massart method [31]. Four grams of chitosan powder were dissolved in 200 mL of (20 %, w/w) acetic acid solution, 6.62 g of $FeSO_4 \cdot 7H_2O$ and 8.68 g of $FeCl_3$ were then added to the biopolymer solution. The mixture was precipitated at 40 °C by addition of 2 M NaOH solution under constant stirring till pH 10-10.4; then the suspension was maintained under continuous agitation for 1 h at 90 °C. The material was washed several times using demineralized water after being collected by decantation and magnetic separation.

(b) Crosslinking of chitosan with epichlorohydrin

MG-CH particles were mixed with alkaline 0.01 M epichlorohydrin solution (in 0.067 M NaOH, corresponding to pH 10) and maintained under agitation for 2 h at 40-50 °C. Unreacted epichlorohydrin was removed by several washing steps after magnetic collection of crosslinked material

(c) Insertion of epichlorohydrin reactive spacer arms (EPI-MG-CH)

Crosslinked MG-CH (wet) was reacted for 3 hours with 15 mL epichlorohydrin in 1:1 ethanol/water solution (150 mL). The activated material (EPI-MG-CH) was obtained after ethanol washing (3 times) and Milli-Q water washing and freeze-drying (after decantation and magnetic separation) (-54 °C, 0.1 mPa).

(d) Insertion of nitrile reactive groups (CN-MG-CH) [26]

An amount of 9.9 g of malononitrile was dissolved in 60 mL of dried DMF (dimethylformamide) before being reacted with 3.4 g of sodium hydride at 60 ± 4 °C for 1 h. After cooling at room temperature, dried EPI-MG-CH micro-particles were dispersed in the reactive media under heating (at 80 ± 4 °C) for 6 h. The material was recovered by decantation and magnetic separation, abundantly rinsed with DMF and finally with Milli-Q water to obtain CN-MG-CH.

(e) Hydrazinyl amine derivative of CE-MG-CH (HA-MG-CH)

Hydrazine hydrate (10.9 g) was dissolved in 30 mL of absolute ethanol before adding CN-MG-CH material; the mixture was maintained under constant stirring for 6 h at 75 ± 2 °C. The sorbent was obtained after decantation and magnetic separation, ethanol washing, Milli-Q water washing and freeze-drying for 24 h (-54 °C, 0.1 mPa) [32, 33], the scheme for sorbent synthesis is shown in Figure 1.

2.3. Sorbent characterization

Different physico-chemical techniques have been used for the characterization of structure and chemical composition of the sorbent [30]. An automatic element analyzer (CHNOS Vario EL III elemental analyzer, Elementar Analysensysteme GmbH, Sonaustraβe, Germany) was used for characterizing the chemical composition of the materials. FTIR spectra were collected using a FTIR-ATR spectrometer (Bruker VERTEX 70 spectrometer, Bruker Optik GmbH, Ettlingen, Germany). Acid-base titration was used for evaluating the content of amine groups in the polymer: the sorbent (100 mg) dispersed in 50 mL (0.05 M HCl solution) overnight was titrated using 0.05 M NaOH solution; the amount of amino groups was quantified by the back-titration of residual HCl concentration. The pH_{PZC} was obtained using the pH-drift method: 100 mg of sorbent was dropped into 50 mL of a 0.1 M NaCl at different initial pH values (pH_0 in the range 1-11); the equilibrium pH (pH_{eq}) was monitored after 48 h

of contact using a Cyber Scan pH 6000, Eutech Instruments Pte, Ltd., Nijkerk, Netherlands. The pH_{PZC} value corresponds to the condition: $pH_0 = pH_{eq}$ [34]. The thermogravimetric analysis of the sorbent was carried out under N_2 atmosphere conditions (in platinum cell). Analysis was performed using a TGA-50/DTA-50/DTG-50 Shimadzu thermogravimetric analyzer (Shimadzu Scientific Instruments, Kyoto, Japan). The temperature ramp was set at 10 °C min^{-1}. Magnetite content was confirmed by weight loss at 650 °C (elimination of organic material). Morphological studies were performed by scanning electron microscopy (Quanta FEG 200, FEI France, Thermo Fisher Scientific, Mérignac, France) while element analysis was obtained using an Oxford Inca 350 EDX microanalyzer (connected to SEM, Oxford Instruments France, Saclay, France). XRD analysis was performed using a Philips PW 3710/31 diffractometer, equipped with a scintillation counter, a Cr-target tube and a Ni filter; analyses were performed under the following conditions: 40 kV and 30 mA. The spectrum was compared with the PDF-2 database for mineral identification.

XPS spectra were collected on an ESCALAB 250XI^+ instrument (Thermo Fischer Scientific, Inc., Waltham, MA, USA) with monochromatic X-ray Al Kα radiation (1486.6 eV) and the following operating parameters: spot size: 500 µm; absolute resolved energy interval calibrated with $Ag3d_{5/2}$ line (0.45 eV) and C1s line (0.82 eV); sample-preparation pressure 10^{-8} mbar; full-spectrum pass energy 50 eV and narrow-spectrum pass energy 20 eV.

2.4. Sorption and desorption tests

Sorption experiments were carried out in batch systems. Working solutions were prepared by dilution of the stock solution with demineralized water and the pH of metal solutions was controlled with 0.1 M/1 M HCl or 0.1 M/1 M NaOH solutions. Metal concentration was systematically analyzed by inductively coupled plasma atomic emission spectrometry (ICP-AES, Horiba – Jobin Yvon Activa M, Longjumeau, France).

Sorption tests were performed by mixing a fixed amount of sorbent (m, g) with a fixed volume (V, L) of metal ion solution (at initial concentration, C_0, mmol L^{-1}) at controlled pH and a rotation speed of 150 rpm. The pH was not controlled but was monitored at the end of the sorption test for verifying that precipitation does not occur during metal sorption. Metal sorption capacity was calculated using the mass balance equation, q (mmol g^{-1}) = (C_0-C_{eq})×V/m; where C_{eq} is the residual metal concentration.

Uptake kinetics were performed by contact of a fixed amount of HA-MG-CH sorbent with 1 L of solution containing either Ni(II) (120 mg Ni L^{-1}) or Pb(II) (150 mg Pb L^{-1}) at pH_0: 5; the sorbent dosage(SD) was set to 250 mg L^{-1} and 200 mg L^{-1} for Ni(II) and Pb(II) experiments, respectively. Samples were collected at fixed times, filtrated and analyzed for plotting the kinetic profiles. For sorption isotherms the initial metal concentration varied in the range 5-300 and 5-500 mg L^{-1} for Ni(II) and Pb(II), respectively (with SD of 170 mg L^{-1} and 140 mg L^{-1}, respectively). High concentration levels were used for evaluating maximum sorption capacities; though they do not correspond to concentration ranges where metal sorption is really competitive. Sorption tests in binary solutions were carried out, at different initial pH values (between 1 and 5) using the same experimental procedures with an equimolar metal concentration (i.e., 0.5 mmol L^{-1}) and a sorbent dosage close to 400 mg L^{-1}. Metal desorption was performed using 0.5 M HCl solution. Contact time for metal sorption was set to 24 h with fixed SD (i.e., 0.344 mg L^{-1} for Ni(II) and 0.364 mg L^{-1} for Pb(II)), metal concentration being set at 196 mg Ni(II) L^{-1} and 129 mg Pb L^{-1} (with pH_0: 5). For desorption steps, the contact time was decreased to 2 h; the SD was 1.7 g L^{-1}. A washing step was operated between each sorption and desorption steps.

2.5. Modeling of sorption processes

Uptake kinetics may be controlled by several diffusion mechanisms, including resistances to bulk, film and intraparticle diffusions, and by the proper reaction rate. Designing micron-sized particles allows reducing the contribution of the resistance to intraparticle diffusion. The Weber and Morris equation ($q(t)=f(t^{0.5})$) is frequently used as a simplified approach for the modeling of resistance to intraparticle diffusion [35]: the linearization of the plot is associated to a control of sorption kinetics by the resistance to intraparticle diffusion; the shift of the ordinate intercept accounts with the contribution of resistance to film diffusion while the co-existence of different linear section is explained by the presence of pores of different sizes in the core of the sorbent. Maintaining a sufficient agitation speed allows reducing the effect of resistance to bulk diffusion (avoiding particle settling) and film diffusion (limiting the thickness of the film). The proper reaction rate is frequently described by the PFORE (pseudo-first order rate equation, [36]) and the PSORE (pseudo-second order rate equation, [37]). Though these equations have been initially developed for modeling homogeneous reactions, they have been extended to the description of kinetics in heterogeneous systems; under these conditions, the rate coefficient should be considered as an apparent constant that intrinsically integrate the relative contribution of diffusion resistances. The relevant equations describing these models are reported in the Additional Material Section (Table AM1).

Sorption isotherms plot the sorption capacity as a function of residual metal concentration; this represents the distribution of solute (i.e., metal ions) between liquid and solid phases at equilibrium and fixed temperature and pH for different initial metal concentrations. The sorption isotherms are commonly described by three equations: the mechanistic Langmuir equation [38, 39], the empiric Freundlich equation [40] and the combined Sips equation (associating Langmuir and Freundlich systems) [41]. These well-known equations are reported in the Additional Material Section (Table AM2).

The selectivity coefficients ($\alpha_{Pb/Ni}$ and $\alpha_{Ni/Pb}$) calculated by the ratio of distribution coefficients $\alpha_{Pb/Ni} = K_d(Pb)/K_d(Ni)$ (and reciprocal), where K_d is calculated as the ratio of sorption capacity at equilibrium to residual metal concentration ($K_d=q_{eq}/C_{eq}$, L g^{-1}). The selectivity coefficients were determined at different pH values by contact of HA-MG-CH with 0.65 mmol L^{-1} equimolar solutions of Pb(II) and Ni(II) (SD: 0.4 g L^{-1}) for 48 h, at room temperature. The final pH was monitored and the residual metal concentrations were determined by ICP-AES; the selectivity coefficients were plotted as a function of equilibrium pH.

The parameters of the different equations were determined by non-linear regression analysis using the Mathematica® software (Wolfram France, Paris, France). The estimated variance was calculated together with the determination coefficient (i.e., R^2) for evaluating the accuracy of experimental fits.

2.6. Tests on complex multi-metal sample and real contaminated stream

A multi-metal solution with an equimolar concentration (i.e., 0.2 mmol L^{-1}) of Al(III), Cd(II), Cu(II), Ni(II), Pb(II) and Cr(VI) was used for testing HA-MG-CH sorption. The initial pH was set to 5; the sorbent dosage was 2.5 g L^{-1}. The residual metal concentrations were measured after 30 min and 60 min of contact; sorption capacities and distribution coefficients were calculated. The equilibrium pH slightly decreased to 4.78.

Another multi-metal solution was collected in the Ataka area (Suez zone), after flooding in December 2017. The pH of the sample was 6.33. Sorption tests were performed at two SD values (i.e., 0.25 and 0.5 g L^{-1}) and samples were collected, filtrated and analyzed at different contact times (i.e., 0.5, 1, 2, 3, 4, and 5 h). Sorption efficiencies, sorption capacities and distribution coefficients were determined for the six metal ions (see above) and the residual concentrations were compared to MCLs (maximum concentration levels) [42].

3. Results and Discussion

3.1. Sorbent characterization

3.1.1. Morphological characterization – SEM & SEM-EDX analysis

Figure AM1 (see Additional Material Section) shows the morphology of sorbent particles before and after metal desorption. The size of sorbent particles ranges between 20 and 60 µm for the majority of sorbent particles; though some smallest objects (micrometric size) can be observed. The surface is irregular and not affected by the treatment (sorption/desorption) applied to the material. The aspect is similar to superimposition of platelets/slabs with small aggregates probably caused to the agglomeration of particles during the co-precipitation of chitosan simultaneously to the synthesis of magnetite (one-pot hydrothermal precipitation of iron(II) and iron(III) precursors in the presence of chitosan). These irregular surfaces contribute to give a relatively large external surface to the material. Figure 2 shows the SEM-EDX surface analysis of the same samples. The presence of iron is directly correlated to the magnetite core; the sorption of Pb(II) and Ni(II) in relevant samples is demonstrated by the appearance of specific peaks. After metal desorption the peaks assigned to Pb(II) and Ni(II) disappear while a new peak appears (corresponding to Cl element): HCl solutions are used for metal desorption and chloride ions bind to protonated reactive groups (N-donor groups). Though the specific surface area (SSA) of this specific sorbent was not determined, similar magnetite/chitosan composite have been characterized with SSA close to 12 ± 2 m^2 g^{-1}.

3.1.2. XRD analysis

XRD analysis was performed on both CN-MG-CH and HA-MG-CH sorbents; Figure AM2 (see Additional Material Section) show poorly resolved patterns. The coating of magnetite with the layer of chitosan (about 61 % of total weight as demonstrated by calcination tests) contributes to the loss of resolution compared to the XRD patterns of pure magnetite. Similar

results were observed with amidoxime-functionalized chitosan [26]; the covering of magnetite surface with a thin layer of organic coating strongly reduces the apparent crystallinity of the composite material. Table AM3 (see Additional Material Section) reports the assignments of the peaks on the XRD patterns for these two materials and their comparison with the reference magnetite material (Fe_3O_4, magnetite mineral phase).

3.1.3. Thermogravimetric analysis – Weight loss

The thermogravimetric analysis of the sorbent is characterized by three steps (Figure AM3**,** see Additional Materials Section) [30, 43, 44]:

(a) from 25.66 °C to 205.5 °C, the sorbent lost about 10.0 %; this fraction corresponds to the amount water sorbed on the material.

(b) from 205.5 °C to 300.8 °C, the weight loss reached 28.2 % (total cumulated loss: 38.2 %); this loss may be attributed to different causes such as the dehydration of the saccharide ring, the partial degradation of the chitosan backbone (organic skeleton of the coating layer), but also to the degradation of amine compounds and relevant functional groups.

(c) from 300.8°C to 801.8 °C, weight variation was 23.3 %; this could be assigned to the thermal degradation of the residual organic fraction but also (to a lesser extent) to the phase change of magnetite core.

Above 800 °C, the total weight loss reached about 61.6 %; this is slightly higher than the weight loss obtained using the calcination method at 650 °C (i.e., 59.7 %). This difference can be explained by the higher temperature (which affects the phase transition of magnetite core) and by the aerobic conditions *vs.* anaerobic conditions for thermal degradation.

3.1.4. Elemental analysis

Elemental analysis was performed at the different stages of the synthesis in order to evaluate the mass percentage of C, H and N elements. In the chitosan-coated magnetite the initial mass

fractions were 15.5 %, 2.9 % and 1.82 % (i.e., 1.30 mmol N g^{-1}), respectively. After nitrilation the composition changed to 22.9 %, 3.65 % and 6.9 % (i.e., 4.93 mmol N g^{-1}), respectively. The variation of nitrogen content (i.e., 3.79 times) exceeds the stoichiometric ratio deduced from expected reaction (i.e., 3 times, Figure 1). This means that the nitrilation is very efficient under selected experimental conditions. The next step in the synthesis consists in the formation of hydrazinyl amine (conversion of nitrile groups,-CN, into -C(NH)$NHNH_2$). The percentages of C, H and N elements changed to: 21.7 %, 7.3 % and 14.4 %, respectively. Nitrogen molar content reached 10.29 mmol N g^{-1}; this is close to 2.1 times the nitrogen content in the intermediary compound. Based on the expected structure of HA-MG-CH, the addition of amine groups in the nitrile intermediary compounds should be close to 3.63 mmol N g^{-1}; assuming a total substitution of nitrile groups with hydrazinyl amine groups would lead to N content close to 12.19 mmol N g^{-1} (i.e., 1.30 + (3*3.63) mmol N g^{-1}). Substitution is not complete on nitrile groups: actually the comparison of nitrogen molar contents shows that substitution yield reached 83 % (i.e., 10.29-1.3=8.99 mmol N g^{-1} compared to 3*3.63=10.89 mmol N g^{-1}). The increase (7.9 times) in nitrogen content between the chitosan/magnetite composite (1.3 mmol N g^{-1}) and HA-MG-CH (10.29 mmol g^{-1}) is higher than expected from theoretical formula (i.e., 7 times). Acid-base titration of the sorbent led to an amino content close to 10.89 mmol N g^{-1}; a little higher than the elemental analysis but of the same order.

3.1.5. FTIR analysis

FT-IR spectrometry was used for characterizing the successive modifications of the material during sorbent synthesis (Figure 3) but also to identify the reactive groups involved in metal sorption (comparison of FT-IR spectra before and after metal sorption) (Figure 4). Spectra are focused on the most representative sections of spectra (full spectra are appearing as Figures AM4-5 in Additional Material Section). The assignments of the peaks that are the most representative of chemical modifications are summarized in Table AM3 (see Additional

Material Section). More specifically, chitosan can be identified through OH (around 3300 cm^{-1}; overlapped with NH stretching vibrations), NH (at 1649 $cm^{-1}$and 1578 cm^{-1}) and C-O (at 1419 cm^{-1} and 1378 cm^{-1}, from residual acetylated moieties of chitin) stretching and bending bands. The grafting of spacing arms is characterized by the formation of C-Cl (methylene chloride: CH_2Cl) with a broad band in the range 630-700 cm^{-1} (and small additional peak at 687 cm^{-1}). The width of this band strongly decreases after hydrazinyl amine grafting; this is a confirmation of the immobilization of new reactive groups on the spacer arms of the modified magnetic/chitosan composite. The grafting of malononitrile moieties on CN-MG-CH intermediary compound is also confirmed by the appearance of nitrile groups at 2360 cm^{-1} (C≡N stretching, reported at 2240-2244 cm^{-1} in the case of amidoximation of poly(acrylonitrile-*co*-acrylic acid) [45] or cellulose [46]). After amidoximation (reaction with hydrazine hydrate) the intensity of the nitrile stretching band strongly decreased indicating the high efficiency of material conversion; similar observations were reported in the case of amidoximated PET derivatives (polyethylene terephthalate functionalized with diaminomaleodinitrile) [47]. The intensity of amine groups was also increased after amidoximation (appearance of new primary and secondary amine groups): the broad band in the range 1630-1550 cm^{-1} confirms this conclusion (compared to CN-MG-CH).

Figure 4 shows the FTIR spectra around 1600 cm^{-1} (representative of amine groups under different environments) for HA-MG-CH before metal sorption, after Pb(II) and Ni(II) sorption and after metal desorption. Indeed, the peak is relatively large corresponding probably to the convolution of different signals associated to the different type of nitrogen-based compounds (primary and secondary amines, imines, etc.) present on the material. The shift of the peak with sorbent modification is then difficult to measure: the differences are not enough marked. Actually the main difference consisted of the enlargement of the full width half maximum (FWHM). While for raw sorbent the FWHM corresponded to about 129 cm^{-1},

it increased to 151 cm^{-1} for Sorbent+Ni(II), 177 cm^{-1} for Sorbent+Pb(II). After metal desorption the FWHM slightly decreased to 146 cm^{-1} (compared to metal-bound materials) but not enough to return to the initial value. This can be explained by the interactions of the nitrogen-based compounds (mainly amine groups) with metal ions. The modification of the environment of amine groups leads to the enlargement of the convoluted bands. The chemical modification is irreversible; the desorption of metal ions made partially free the amine groups but the acid solutions contributes to the change in the width of the convoluted amine band.

3.1.6. Titration analysis – pH_{PZC}

Figure AM6 (see Additional Material Section) shows the titration curve for the determination of the pH_{PZC} (pH-drift method). The maximum pH variation is reached at pH_0=4 (i.e., ΔpH=2.3). The ΔpH is equalized to 0 for pH_{PZC}=7.87. This means that in the whole pH range used for the study of Pb(II) and Ni(II) sorption, the surface of the sorbent is positively charged. This positive charge is attractive for anion binding; however, in the case of metal cations protonated N-based reactive groups may have repulsive effect for cation binding. Obviously, as the pH increases the repulsive effect becomes progressively negligible. The presence of two primary amine groups and one secondary amine group on the hydrazinyl moiety confers to the sorbent basic properties. Williams [48] reported the pK_a values of a series of hydrazine derivatives: their pK_a values (for N-based groups) stand between 6.3 and 8.1, depending on the type of substituent. This is consistent with the pH_{PZC} obtained by titration.

3.1.7. XPS characterization of sorbent-metal interaction

The XPS characterization of the interactions between the sorbent and Pb(II) and Ni(II) sorption is discussed in detail in the Additional Material Section (see Figure AM7, Tables AM and AM6 and relevant comments). The analysis of the XPS in the area representative of C-

based reactive groups shows a great diversity of bands and chemical environments (Table AM5, see Additional Material Section). Table AM6 reports the assignments of the relevant binding energies: (a) 284.04 eV for C-C or C-H; (b) 285.67 eV, mainly assigned to C-NH and C-NH_2 chemical bonds; (c) 287.46 eV for C(-O, =N), and (d) 287.9 eV for O-C-O at 287.9 eV [49-52]. Though the change in the chemical environment due to metal binding could shift these specific binding energies, the sorption of Pb(II) and Pb(II) hardly affect the XPS spectra around C element: the binding of metal ions is mainly located on other reactive groups; including (mainly) N-based reactive functions and (to a lesser extent) O-based functions.

Tables AM5 and AM6 (see Additional Material Section) show the peak around 532.7 eV, which is assigned to C-O, O-H or bound water. Oxygen element is also appearing in the sorbent under the inorganic form (due to magnetite core): the peak at 530.0 eV is attributed to lattice oxygen in Fe_3O_4,; it is similar to the value of the binding energy for macro-scaled crystallite of magnetite, while the peak found at 529.5 is assigned to Fe_2O_3 [53-57]. In the case of metal-loaded sorbent, new O-based peaks correspond to the binding energies of -O-Ni and -O-Pb at 631.58 eV and 530.39 eV, respectively. The O1s binding energies representative of iron oxide and C-O, OH groups are hardly affected by metal sorption. This means that the O-based reactive groups on the sorbent are poorly contributing to metal binding.

The spectrum of N1s band for the sorbent shows three peaks (Tables AM5 and AM6; Additional Material Section): at 397.7 eV (assigned to NH-NH2 or =NH-N- bonds, in the hydrazinyl amine derivative), at 399.3 eV (assigned to C–N or NH_2 chemical bonds), and at 400.0 eV (associated to amine groups in the ammonium form, NH_3^+) [58, 59]. The sorption of metal ions affects the environment of amine groups whose binding energies are slightly shifted toward For loaded sorbent these peaks appeared at 397.75 eV, 399.34 eV and 400.34 eV, respectively; for Ni(II). In the case of Pb(II) the BEs were are shifted to while for Pb, it

assigned at 398.12 eV, 400.21 eV, and 400.7 eV, 398.12 eV, respectively. It is noteworthy that a new peak (assigned to amine metal bonding) is appearing at 398.49 eV for Ni(II) sorption, and 398.88 eV for Pb(II) sorption.

The XPS analysis of the Fe 2p core level shows that the metal may appear under different oxidation states [60, 61]. Main differences between different iron oxides are located in the region around 720 eV where the satellite peak associated to the $Fe2p_{3/2}$ band is appearing and in the region around 707 eV where differences between Fe(II) and Fe(III) can be identified [62]. The Fe 2p XPS spectrum is shown in Tables AM5 and AM6 and on Figure AM7 (sees Additional Material Section). Iron is identified under two oxidation states: Fe^{2+} is present under octahedral form while Fe^{3+} is found under both octahedral and tetrahedral sites [57]. After metal sorption, the 4f peak for lead and 2p peaks for nickel are clearly identified [63]. High resolution XPS spectra of sorbent before and after metal sorption reveal the bonding of metal ions through N reactive groups on the hydrazinyl amine and O reactive groups either present on the epichlorohydrin spacer arm or on the chitosan moieties. This may explain the high efficiency of this sorbent for metal binding, especially under slightly acidic solution.

3.2. Sorption properties

3.2.1. Effect of pH on metal sorption – Interpretation of sorption mechanisms

The pH has a strong impact on metal sorption properties due to different effects associated to metal speciation (hydrolyzed species, for example) and to the physico-chemical characteristics of sorbent surface (protonation/deprotonation of functional groups). Figure 2a shows the effect of equilibrium pH on Pb(II) and Ni(II) sorption using HA-MG-CH sorbent. The two metal ions have a similar behavior: the pH-profiles of sorption capacities are almost overlapped. Below pH 3, the sorption capacities remain in the range 0.15-0.25 mmol g^{-1} for both Pb(II) and Ni(II). Under these conditions, far below the pH_{PZC} (i.e., 7.87), the sorbent is

protonated. The strong protonation of amine functions is supposed to limit sorption performance: the protonated groups repulse metal cations. However, the results show that a non-negligible sorption occurs; this is probably due to the binding of neutral metal species (under the form of sulfate complexes)..With the pH increase the protonation of amine groups progressively decreases and the sorption of both Pb(II) and Ni(II) increases almost linearly up to pH 6 where the sorption tends to stabilize. Metal ions are bound by chelation to amine groups. In the case of lead, hydrolysis phenomena may affect the solubility of the metal above 5.5 (depending on metal concentration); this phenomenon is less marked for Ni(II). For limiting the risk to attribute sorption performance to precipitation the pH value for further studies was set at 5. This is especially important because the sorption is followed by a pH increase, which is illustrated by Figure 2b. The profiles for Pb(II) and Ni-(II) are very close in terms of pH changes: (a) at pH 1, the pH changes are relatively limited (below 0.2 pH unit), (b) in the range pH 2-5, the pH increases during metal sorption by 0.5-0.8 unit, and (c) at pH above 6 the pH tends to stabilize close to the initial pH value. The pH variations are much less marked than the pH values observed during the study of pH_{PZC} (Figure AM6, see Additional Material Section), where the pH variation could reach up to 2.2 units. The binding of metal cations reduces the binding of protons on amine groups;the potential to protonate amine groups is decreased and then the pH variation is minimized.

Figure AM8a (see Additional Material Section) shows the sorption efficiency as a function of equilibrium pH: the sorption efficiency remained below 80 %, this means that experimental conditions have been appropriately selected for clearly illustrating the limiting effect of pH on the complete pH range. Figure AM8b shows the log-plots of distribution coefficient vs equilibrium pH. The distribution coefficient represents the ratio of sorption capacity to equilibrium metal concentration ($K_d=q_{eq}/C_{eq}$, L g^{-1}). The slope of the linearized curves are close to 0.3 (i.e., 0.33 for Pb(II) and 0.27 for Ni(II)). In the case of systems driven by ion-

exchange mechanisms this is frequently associated to the number of protons that are exchanged with metal ions. This is not the case here, at least in this pH range.

3.2.2. Uptake kinetics – controlling steps

The uptake kinetics are reported in Figure 3. Under selected experimental conditions a contact time of 15 min is sufficient for reaching the equilibrium for Pb(II); Ni(II) binding is little slower since the equilibrium is achieved within 40 min. The sorption is decomposed in two phases; (a) the initial step lasts for 5-8 min and represents the instantaneous sorption on external reactive sites (about 90 % of total sorption for Pb(II) and 50 % for Ni(II)), and (b) the second step that is associated to sorption on internal reactive groups (within the modified chitosan layers that are deposited at the surface of magnetite core). The contribution of this second step is negligible for Pb(II) but counts for 50 % in the case of Ni(II). This is confirmed by the fractional approach to equilibrium ($q(t)/q_{eq}$) when plotted as a function of contact time (Figure AM9a, see Additional Material Section).

The kinetic profiles are modeled using the PFORE (Figure 3a) and the PSORE (Figure 3b) using the parameters summarized in Table 1. Both the PFORE and the PSORE give relatively good fit of experimental profiles. However, the application of the PFORE gives a little better correlation (based on estimated variance (EV) and R^2 values); in addition, the comparison of calculated and experimental values for the equilibrium sorption capacities demonstrates that PSORE overestimated the equilibrium sorption capacities, while the PFORE perfectly fitted these experimental values for both Pb(II) and Ni(II). Simonin [64] commented on the statistical effect of experimental point distribution on the accuracy of kinetic modeling and more specifically the appropriateness of model selection in the fit of experimental data. He observed that using points close to the equilibrium forces the modeling to the PSORE against PFORE. The sorption capacities at equilibrium reach 3.88 mmol Ni g^{-1} and 2.20 mmol Pb g^{-1}

(under selected experimental conditions). The apparent kinetic coefficient is about 4 times higher for Pb(II) compared to Ni(II) (i.e., 36.2×10^{-2} min^{-1} vs. 8.91×10^{-2} min^{-1}). This is consistent with the comparison of kinetic profiles and times required for reaching the equilibrium. The comparison of the ionic radii for Pb(II) and Ni(II) (under their hexa-hydrated forms) (i.e., 1.19-1.2 Å and 0.69-.715 Å, respectively, [65]) is not consistent with the fastest kinetics of Pb(II) sorption. This could be explained by the limitation of sorption to the external layers of the sorbent. On the opposite hand, Marcus [66] reported the diffusivities of metal ions in water: 5.67×10^{-8} m^2 min^{-1} and 3.97×10^{-8} m^2 min^{-1} for Pb(II) and Ni(II), respectively. Despite a higher hydrated ionic radius, lead cations have a higher diffusivity than Ni(II) in water. Figure AM9b (see Additional Material Section) plots sorption capacity as a function of the square root of contact time; this is the so-called Morris & Weber model designed for approaching the kinetic profiles of systems controlled by intraparticle diffusion. A linear plot means that the uptake kinetics is controlled by the resistance to intraparticle diffusion. When the plot is represented by different linear sections, this is associated to different regimes of intraparticle diffusion (due to different porous systems). When the plot does not pass through the origin, this is generally associated to an important contribution of resistance to film diffusion. Here the plot does not pass through the origin: the resistance to film diffusion cannot be neglected. In the case of Ni(II) a single linear section can be detected between 0 and 6 $min^{0.5}$ (i.e., 40 min). In the case of Pb(II) the initial fast sorption takes place within 10 min of contact (i.e., 3 $min^{0.5}$) while a second step, with a much slower slope, lasts till 30 min of contact (probably associated to the resistance to intraparticle diffusion through the thin layers of modified chitosan).

The sorption of Pb(II) and Ni(II) is relatively fast; contact times lower than 15-45 min are sufficient for reaching equilibrium under selected experimental conditions. The micron-size of

sorbent particles and the deposition of a thin layer of modified chitosan on the magnetite core can explain these fast kinetic characteristics.

3.2.3. Sorption isotherms – maximum sorption capacities and metal affinities

Sorption isotherms have been determined at pH 5 (Figure 4). For Pb(II), the curve shows a steep initial slope followed by an equilibrium plateau reached at a residual metal concentration close to 0.5 mmol Pb L^{-1}. The maximum sorption capacity corresponds to 2.63 mmol Pb g^{-1}. In the case of Ni(II), the initial slope is less steep but the sorption capacity progressively increases and reaches a much higher maximum sorption capacity, close to 3.9 mmol Ni g^{-1}. Yang and Alexandratos [67] investigated the affinity of a series of sorbent bearing different donor atoms for the extraction of lanthanides. They reported that the Hard and Soft Acid and Base theory (the so-called Pearson's rules, [68]) is driving the affinity of ligands for metal ions; however, they also commented that other parameters may influence the interaction between ligands and metals ions such as the effect of counter-anion coordination, the protonation of the ligand and hydration. The complexation of metal ions competes with hydration: water coordinates to ions in solution, affecting their interaction with ligands on the sorbent [67]. The "strength" of hydration can be measured by the dehydration enthalpy; Marcus [66] reported values of -2119 kJ mol^{-1} and -1572 kJ mol^{-1} for the hydration enthalpies of Pb(II) and Ni(II), respectively. This means that in terms of dehydration enthalpy the hydration coordination is stronger with Pb(II) than with Ni(II). The affinity coefficients (*b* coefficient in the Langmuir equation, also correlated to initial slope for sorption isotherms) are not consistent with this ranking; this probably means that other factors are influencing more significantly metal binding. The polarizability and softness parameters of lead (i.e., 11.9 cm^3 mol^{-1}, and 0.41, respectively) are much higher than the values for Ni(II) (i.e., 1.6 cm^3 mol^{-1}, and -0.11) [66]. The highest polarizability of Pb(II) makes these ions preferentially bound to ligands containing N as donor atoms (like in the hydrazinyl group). Giraldo et al.

[69] explain the better sorption of Pb(II) over Cu(II) , Cd(II) and Zn(II) metal cations on gelatin/activated carbon beads by its highest ionic radius, while Yang et al. correlates the better affinity of thiourea/hypercrosslinked polystyrene for Pb(II) over Cd(II) and Cu(II) to the smallest hydrated radius [70].

Figure 7 shows the fits of sorption isotherms with the Langmuir, the Freundlich and the Sips equations. Table 2 summarizes the parameters of these models (together with the estimated variances, EV, and the determination coefficients, R^2). The Freundlich equation being of power-type, this model is poorly consistent with the asymptotic profile of sorption isotherms. This is confirmed by the comparison of statistical parameters in Table 2, at least for Ni(II); in the case of Pb(II) the comparison of experimental profiles and fitted curves is more difficult to establish due to the specific shape of the curve (quasi-irreversible isotherm). The mechanistic equation of Langmuir correctly fits Ni(II) sorption isotherm but fails to describe Pb(II) curve. On the other hand the Sips equation gives a good mathematical fit of experimental profiles because of the introduction of a third fitting parameter but at the expense of a loss in physico-chemical sense. In addition, the maximum sorption capacity at monolayer saturation (i.e., q_m) is significantly overestimated while with the Langmuir equation the estimated q_m values are more consistent with the experimental values. The affinity coefficients (*b* parameter of the Langmuir equation) are consistent with the highest initial slope of the sorption isotherm for both Pb(II) (i.e., 35.2 L $mmol^{-1}$) compared to Ni(II) (i.e., 2.64 L $mmol^{-1}$); contrary to the coefficients determined by the Sips equation (Table 2).

Table 3 reports the sorption properties of a series of sorbents for Pb(II) and Ni(II). Though the comparison is generally difficult because the experiments were not systematically carried out under similar processing conditions, the table shows that HA-MG-CH is among the most efficient sorbents for both Pb(II) and Ni(II). Some synthetic resins show much higher sorption capacities: for example synthetic resins like D151 macroporous weak acid resin or chitosan

grafted with acrylic acid for Ni(II) with maximum sorption capacities higher than 5 mmol Ni g^{-1} [71, 72], or thiourea-modified polystyrene-based resin for Pb(II) (up to 3.33 mmol Pb g^{-1}) [70].

The sorbent has a higher sorption capacity for Ni(II) compared to Pb(II). However, the affinity coefficient (correlated to the initial slope of the isotherm curve) is greater for Pb(II) than for Ni(II).. It is important to verify if the sorption process can be used for separating the two metal ions. The selectivity was evaluated as a function of pH (Figure 8). Acidic solutions are more favorable to Ni(II) binding with a selectivity coefficient $\alpha_{Ni/Pb}$ that exceeds 33 at pH 1.2 (with a cumulative sorption capacity close to 1 mmol metal g^{-1}; Ni(II) represent about 81 % of total bound metal). On the opposite hand, at pH 6.5, the sorbent is enriched with Pb(II): the selectivity coefficient $\alpha_{Pb/Ni}$ reaches 24; the cumulative sorption capacity increases to 2.74 mmol metal g^{-1} (constituted of 47 % of Ni(II) and 53 % of Pb(II)). The differences in the affinities of HA-MG-CH for Pb(II) and Ni(II) allows enriching the solid phase with Ni(II) in acidic solutions but not enough for efficiently separating the two metals.

The affinity of a sorbent for metal ions is controlled by intrinsic sorbent characteristics (protonation/deprotonation), proper speciation of the metal, but also characteristics as the hydrated size of the metal ions, their ionic radius, their charge and their electronegativity. Ionic parameters (electronegativity ionic size) control the polarizability of the metal ions and then their interaction with ligands. The hard and soft acid and base theory (HSAB, [68]) established that hard acids react preferentially (both in terms of thermodynamic and kinetic parameters) with hard bases (and reciprocally: soft acids with soft bases). The softness parameters for Ni(II) and Pb(II) are respectively close to -0.11 and +0.41, respectively [66]. These two metal ions are generally classified as borderline metals (intermediary compounds) though Pb(II) is closer to the limit corresponding to soft acids (such as N-based donor ligands) than Ni(II). Soft acids are preferentially bound to soft bases such as N-based donor ligands.

As a consequence Pb(II) is supposed to be more strongly bound to soft ligands than Ni(II). The sorbents is characterized by several types of amine/hydrazine groups that can be characterized as hard acids. Ones would consequently expect that Ni(II) would be more strongly bound to the sorbent than Pb(II). This is the case while comparing the sorption capacities ($q_{m,exp}$= 3.90 mmol Ni g^{-1}, compared to Pb(II); i.e., $q_{m,exp}$= 2.63 mmol Pb g^{-1}) but not the affinity coefficients (b_L= 3.90 L $mmol^{-1}$ for Ni(II), and b_L= 35.2 L $mmol^{-1}$ for Pb(II)) for single metal concentrations (Figure 7). In the case of bi-component equimolar solutions, the preference is modulated by the pH (and the protonation of reactive groups)(Figure 8). At pH lower than 3.5 the expected order of priority is consistent: the sorbent has a preference for Ni(II); this trend is reversed when the pH increases above pH 3.5: the sorbent preferentially binds Pb(II). This is probably associated to different protonation rates of the different N-based reactive groups. The deprotonation of some reactive changing the preference of the sorbent for target metals through the effect of changes in the apparent softness of these reactive groups. Alexandratos and Zhu [73] reported the impact of acid base properties of a family of phosphate-based ligands on the affinity of sorbents for metal binding: this effect is modulated by the type(base metal vs. rare earth element) and charge of metal ions (divalent vs. trivalent). The highest sorption of Ni(II) (compared to Pb(II) in single-metal solutions can be also partially explained by the difference in the hydrated radius of metal ions (i.e., 1.20 Å and 0.71 Å, for Pb(II) and Ni(II), respectively): smaller hydrated species being more efficiently bound on the sorbent.

3.2.4. Metal desorption and sorbent recycling

The competitiveness of a sorption process must take into account not only sorption properties but also the efficiency of metal recovery (for final removal and/or valorization) and the effectiveness of sorbent recycling. Though complexing agents may be used for metal desorption from loaded sorbents, this generally means more expensive processing and

complex valorization of metal from eluates. For this reason, preferred processes usually apply pH changes for metal desorption. In the case of HA-MG-CH the study of pH effect on sorption performance clearly demonstrated the critical impact of pH: deprotonation of reactive nitrogen-based groups is required for efficient binding of metal cations. As a consequence, favoring the protonation of the metal-loaded sorbent is expected to facilitate the reversibility of metal binding. Logically, weakly concentrated acid solutions have been tested in order to prevent degradation of the sorbent. The solubility of metal salts is also a parameter to be taken into account and in the case of Pb(II) and Ni(II), HCl solution was selected for investigating metal desorption. Long exposure to drastic acid solutions may also cause damages to the polymer coating or to the magnetic core. Though the concentration of iron in the eluate was not analyzed, the EDX analysis of the surface of sorbent after metal leaching did not show significant changes. The relative stabilities of the sorption and desorption performances over the five cycles confirm the global stability of the material. This is consistent with results obtained with other magnetite/chitosan based composites. The coating of the magnetite core with chitosan may contribute to stabilize its in acidic solutions for short contact times; though a partial dissolving cannot be rejected. In order to evaluate the required time for efficient desorption a preliminary study of the kinetics of desorption was performed (Figure AM10, see Additional Material Section). A few minutes of contact (i.e., 2-3 min) with a 0.5 M HCl solution are sufficient for achieving more than 98 % of lead desorption; full desorption is readily reached contrary to nickel that requires much longer contact time. Indeed, after 2 min of contact nickel desorption does not exceed 90 % and desorption efficiency progressively increases and complete desorption requires 60 min of contact. There is a kind of "symmetry" between the phenomena of sorption and desorption that are both faster with Pb(II) than with Ni(II). In the case of uranyl species adsorbed on two types of silica gel particles the sorption kinetics were controlled by the size of pores [74]: microporous silica gel lasted longer time for

the binding of polynuclear hydrolyzed uranyl species of large ionic size compared to mesoporous silica gel while the acidic desorption of uranyl species displaced the speciation of metal toward the formation of free uranyl species; their smaller ionic size enhanced diffusion properties and the desorption showed similar kinetic profiles for the two kinds of silica gel particles. In the present case this size effect is not controlling (or marginally) mass transfer properties since selected metal ions are not forming polynuclear or large ionic size species. A contact time of 60 min was used for further tests on the recycling of the sorbent.

Table 4 compares the average values of sorption/desorption efficiencies and sorption capacities for Pb(II) and Ni(II) recovery using HA-MG-CH for 5 successive cycles. There is a small and continuous decrease in sorption capacities along the 5 cycles for both Ni(II) and Pb(II). However, the total decrease does not exceed 8 % for Ni(II) and even less for Pb(II) (i.e., less than 5 %). On the other hand, the average desorption efficiency over the 5 cycles reaches 98.4 % (± 2.0 %) for Ni(II) and 97.5 % (± 1.3 %) for Pb(II). This means that globally both the sorption and the desorption performances are remarkably stable for a minimum of 5 cycles. The metal can be readily desorbed with 0.5 M HCl solution and the sorbent efficiently reused.

3.2.5. Tests on complex multi-metal sample and real contaminated stream

For the evaluation of the performance of a sorption system it is necessary to test its "robustness" through the study of sorption performances in complex solutions; i.e., multi-metallic solutions and real effluents or wastewater. Table 5 reports the sorption efficiencies, sorption capacities and distribution coefficients (i.e., K_d, L g^{-1}) of HA-MG-CH at 30 min and 60 min for 6 metal ions (including Pb(II) and Ni(II)), at equimolar concentrations (i.e., 0.2 mmol L^{-1}). First, the sorption efficiency is considerably improved while increasing the contact time from 30 min to 60 min. This is consistent with kinetic studies; the complex composition

of the solution (and more specifically the total multi-metal concentration) may explain the more marked effect of contact time. After 60 min of contact 4 of the 6 metal ions show a high removal efficiency (i.e., Pb(II), Cu(II), Cd(II) and Ni(II), greater than 90 %) while for Al(III) and Cr(VI) removal efficiencies are much lower (i.e., 38 % and 58 %, respectively). The comparison of distribution coefficients allows ranking the metal ions in terms of affinity for HA-MG-CH: Pb(II) >> Cu(II) > Cd(II) ≈ Ni(II) >> Cr(VI) ≈ Al(III). Al(III) is classified in hard acid family, contrary to Pb(II), Ni(II), Cu(II) (borderline acids) and Cd(II) (soft acid); they have more affinity for hard and borderline base including N-bearing functional groups). A selectivity coefficient $\alpha_{Pb/metal}$ can be defined as the ratio $K_d(Pb)/K_d(metal)$. The preference of HA-MG-CH for Pb(II) over the other metals is marked against Al(III) ($\alpha_{Pb/Al}$ = 39.6) and Cr(VI) ($\alpha_{Pb/Cr}$ = 17.6) and less significant against Cu(II), Cd(II) and Ni(II) ($\alpha_{Pb/metal}$: 2.6, 2.4 and 1.8, respectively). The cumulative sorption capacity at 60 min contact time reaches 2.36 mmol metal g^{-1}; this is consistent with the order of magnitude of the sorption capacities obtained in the sorption isotherms for Ni(II) and Pb(II) sorption for residual (individual) metal concentration close to 0.274 mmol metal L^{-1} (i.e., the value of the cumulative molar concentration of the 6 metal ions): 1.82 mmol Ni g^{-1} and 2.28 mmol Pb g^{-1} (Figure 7). HA-MG-CH has a preference for Pb(II) but not sufficient for providing a sufficient selectivity for separation purposes. The sorbent has a large spectrum of interactions. It is noteworthy that for multi-metal solutions at equimolar concentrations, it was not possible establishing a correlation between the softness parameter and the distribution coefficients (K_d).Several different mechanisms with cross effects can differently affect the sorption affinity of amine and hydrazide groups for target metal ions (as reported above).

Figure AM11 shows that the values of dehydration enthalpies of metal cations roughly align along the effective sorption capacities obtained from equimolar multi-metal solution. Chromate anions (Lobe-HOMO Lewis base, weak base) are logically following a different

trend since another mechanism is probably involved; metal anions can be bound on protonated amine groups in acid solutions.

The treatment of a stormwater sample was also performed using HA-MG-CH; Tables 6 and 7 summarize the results obtained for the purification of this metal-contaminated water. Six metal ions have been considered (the same that were carried out above). The effect of the complexity of the water sample was compensated by testing longer contact times (up to 5 h) and different sorbent dosages with different objectives: (a) calculating the sorption efficiency, (b) determining the affinity order (based on K_d values), and (c) evaluating the possibility to reach drinking water standards (WHO [42]) for selected metal ions. Based on the composition of water sample and the WHO regulations a contact time of 5 hours is sufficient at a sorbent dosage of 250 mg L^{-1} for achieving target levels, except for Pb(II). While increasing the SD to 500 mg L^{-1}, the contact time required to reach limit values is 2 hours. For most of selected metal ions after 5 h of contact more the sorption efficiency approaches or exceeds 95 %, with the remarkable exception of Cr(VI) (which is at a relatively low value, i.e., 1.54 µmol Cr L^{-1} or 0.08 mg Cr L^{-1}): sorption efficiency reaches only 50 %. Increasing the sorbent dosage hardly changes the sorption efficiency for the different metal ions at 5 h of contact time. The distributions coefficients can be ranked according to:

SD: 250 mg L^{-1} – Pb(II) >> Al(III) > Cu(II) > Cd(II) > Ni(II) >> Cr(VI)

SD: 500 mg L^{-1} – Pb(II) >> Al(III) > Cu(II) > Cd(II) ≈ Ni(II) >> Cr(VI).

These results confirm the preference for Pb(II) over other divalent or trivalent metal cations. HA-MG-CH is capable of purifying this stormwater contaminated with variable concentrations of selected heavy metal ions.

4. Conclusion

The grafting of hydrazinyl-amine functions on chitosan backbone (immobilized at the surface of magnetite particles generated *in situ*) allows synthesizing a sorbent (HA-MG-CH) very efficient for the recovery of lead (preferentially to nickel). The magnetic core allows readily recovering the material at the end of the sorption.

The successive steps of the chemical modification of magnetic chitosan micro-particles are confirmed by the elemental analysis and the FT-IR spectrometry analysis of the materials. SEM and SEM-EDX analyses allow characterizing the surfaces and the effective sorption of metal ions at the surface of HA-MG-CH sorbent.

The study of pH effect on metal sorption shows the substantial increase of sorption capacity with the deprotonation of amine groups (pH_{PZC} of HA-MG-CH close to 7.87). Uptake kinetics is relatively fast: a contact time of 15-45 min is generally sufficient for reaching the equilibrium under selected experimental conditions (depending on the metal). The pseudo-first order rate equation fits well kinetic profiles. High sorption capacities are obtained at pH 5: up to 4.3 mmol Ni g^{-1} and 2.5 mmol Pb g^{-1}. The Sips equation accurately fits sorption isotherms. The study of metal sorption in bi-component solutions confirms the preference of the sorbent for Pb(II) over Ni(II); the selectivity is controlled by the pH: the sorbent being even more selective for Pb(II) at acidic pH values (though the sorption capacity is decreased). In multi-metal equimolar solutions, the sorbent shows a preference for Pb(II) > Cu(II) > Ni(II) ≈ Cd(II) > Cr(VI) ≈ Al(III) (based on the comparison of distribution coefficients, K_d).

Metal desorption is efficiently performed using 0.5 M HCl solutions: desorption kinetics is fast (15-30 minutes are sufficient). The recycling of the sorbent over 5 sorption/desorption cycles shows a slight decrease in sorption capacity at the fifth cycle (about 8 %) while the average desorption for both Pb(II) and Ni(II) exceeds 97 %.

The tests performed on stormwater show the efficiency of the sorbent for decreasing the residual concentrations of target metal ions below the maximum allowable concentration levels for drinking water (according World Health Organization).

Acknowledgements

The authors acknowledge the French government (through Institut Français d'Egypte), and China Science and Technology Exchange Center (CSTEC) through Talented Young Scientistes Program (TYSP) for the post-doc fellowships of Mohammed F. HAMZA. They are also grateful for IFE and Egyptian academy of scientific research and technology for funded IMHOTEP project (Metal Valor). Authors also thank the technical support of Thierry Vincent, André Brun (C2MA, IMT – Mines Ales) and Eryuan Wei, Innovation Center for Metal Resources Utilization and Environment Protection (Guangxi University).

References

[1] M.M. Matlock, B.S. Howerton, D.A. Atwood, Irreversible precipitation of mercury and lead, J. Hazard. Mater., 84 (2001) 73-82.
[2] D. Kavak, Removal of lead from aqueous solutions by precipitation: statistical analysis and modeling, Desalin. Water Treat, 51 (2013) 1720-1726.
[3] M.K. Jha, D. Gupta, P.K. Choubey, V. Kumar, J. Jeong, J.-c. Lee, Solvent extraction of copper, zinc, cadmium and nickel from sulfate solution in mixer settler unit (MSU), Sep. Purif. Technol., 122 (2014) 119-127.
[4] L.Y. Wang, M.S. Lee, Recovery of Co(II) and Ni(II) from chloride leach solution of nickel laterite ore by solvent extraction with a mixture of Cyanex 301 and TBP, J. Mol. Liq., 240 (2017) 345-350.
[5] R.N.R. Sulaiman, N. Othman, Synergistic green extraction of nickel ions from electroplating waste via mixtures of chelating and organophosphorus carrier, J. Hazard. Mater., 340 (2017) 77-84.
[6] M. Monier, A.L. Shafik, D.A. Abdel-Latif, Synthesis of azo-functionalized ion-imprinted polymeric resin for selective extraction of nickel(II) ions, Polym. Int., 67 (2018) 1035-1045.
[7] A. Lalmi, K.-E. Bouhidel, B. Sahraoui, C.E.H. Anfif, Removal of lead from polluted waters using ion exchange resin with $Ca(NO_3)_{(2)}$ for elution, Hydrometallurgy, 178 (2018) 287-293.
[8] N. Chanthapon, S. Sarkar, P. Kidkhunthod, S. Padungthon, Lead removal by a reusable gel cation exchange resin containing nano-scale zero valent iron, Chem. Eng. J., 331 (2018) 545-555.
[9] P. Abbasi, B. McKevitt, D.B. Dreisinger, The kinetics of nickel recovery from ferrous containing solutions using an Iminodiacetic acid ion exchange resin, Hydrometallurgy, 175 (2018) 333-339.

[10] K. Ohto, S. Inoue, N. Eguichi, T. Shinohara, K. Inoue, Adsorption behavior of lead ion on calix 4 arene tetracarboxylic acid impregnated resin, Sep. Sci. Technol., 37 (2002) 1943-1958.
[11] F.T. Mu, Q. Jia, Y.M. Tian, Q.K. Shang, Extraction of cobalt(II) and nickel(II) by a solvent impregnated resin containing bis(2,4,4-trimethylpentyl)monothiophosphinic acid, Adsorption, 14 (2008) 31-36.
[12] S.Y. Bao, K. Li, P. Ning, J.H. Peng, X. Jin, L.H. Tang, Highly effective removal of mercury and lead ions from wastewater by mercaptoamine-functionalised silica-coated magnetic nano-adsorbents: Behaviours and mechanisms, Appl. Surf. Sci., 393 (2017) 457-466.
[13] S. Zhang, F. Xu, Y.F. Wang, W.Z. Zhang, X.L. Peng, F. Pepe, Silica modified calcium alginate-xanthan gum hybrid bead composites for the removal and recovery of Pb(II) from aqueous solution, Chem. Eng. J., 234 (2013) 33-42.
[14] E. Aranda-Garcia, E. Cristiani-Urbina, Kinetic, equilibrium, and thermodynamic analyses of Ni(II) biosorption from aqueous solution by acorn shell of *Quercus crassipes*, Water Air Soil Pollut., 229 (2018) 17.
[15] Y.N. Mata, M.L. Blazquez, A. Ballester, F. Gonzalez, J.A. Munoz, Biosorption of cadmium, lead and copper with calcium alginate xerogels and immobilized *Fucus vesiculosus*, J. Hazard. Mater., 163 (2009) 555-562.
[16] R. Tabaraki, A. Nateghi, S. Ahmady-Asbchin, Biosorption of lead (II) ions on *Sargassum ilicifolium*: Application of response surface methodology, Int. Biodeterior. Biodegrad., 93 (2014) 145-152.
[17] R.A. Muzzarelli, O. Tubertini, Chitin and chitosan as chromatographic supports and adsorbents for collection of metal ions from organic and aqueous solutions and sea-water, Talanta, 16 (1969) 1571-1577.
[18] E. Guibal, Interactions of metal ions with chitosan-based sorbents: a review, Sep. Purif. Technol., 38 (2004) 43-74.
[19] L.T. Busuioc, C.M. Simonescu, R.E. Patescu, C. Onose, Removal of lead(II), nickel(II), zinc(II) and copper(II) from multi-metal systems by chitosan-glutaraldehyde beads, Rev. Chim., 67 (2016) 2504-2510.
[20] S. Jeremic, T.H. Tran, Z. Markovic, T.C. Ngo, D.Q. Dao, Insight into interaction properties between mercury and lead cations with chitosan and chitin: Density functional theory studies, Comput. Theor. Chem., 1138 (2018) 99-106.
[21] W.S. Wan Ngah, C.S. Endud, R. Mayanar, Removal of copper(II) ions from aqueous solution onto chitosan and cross-linked chitosan beads, React. Funct. Polym., 50 (2002) 181-190.
[22] L. Sheng, L. Zhou, Z. Huang, Z. Liu, Q. Chen, G. Huang, A.A. Adesina, Facile synthesis of magnetic chitosan nano-particles functionalized with N/O-containing groups for efficient adsorption of U(VI) from aqueous solution, J. Radioanal. Nucl. Chem., 310 (2016) 1361-1371.
[23] J.d. Santos Menegucci, M.-K.M.S. Santos, D.J.S. Dias, J.A. Chaker, M.H. Sousa, One-step synthesis of magnetic chitosan for controlled release of 5-hydroxytryptophan, J. Magn. Magn. Mater., (2015).
[24] F.P. Zhao, E. Repo, M. Sillanpaa, Y. Meng, D.L. Yin, W.Z. Tang, Green synthesis of magnetic EDTA- and/or DTPA-cross-linked chitosan adsorbents for highly efficient removal of metals, Ind. Eng. Chem. Res., 54 (2015) 1271-1281.
[25] A.A. Galhoum, A.A. Atia, M.G. Mahfouz, S.T. Abdel-Rehem, N.A. Gomaa, T. Vincent, E. Guibal, Dy(III) recovery from dilute solutions using magnetic-chitosan nano-based particles grafted with amino acids, J. Mater. Sci., 50 (2015) 2832-2848.

[26] M.F. Hamza, J.-C. Roux, E. Guibal, Uranium and europium sorption on amidoxime-functionalized magnetic chitosan micro-particles, Chem. Eng. J., 344 (2018) 124-137.
[27] G.R. Mahdavinia, E. Shokri, Synthesis and characterization of magnetic amidoximated chitosan-g poly (polyacrylonitrile)/laponite RD nanocomposites with enhanced adsorption capacity for Cu^{2+}, Turk. J. Chem., 41 (2017) 135-152.
[28] E.A. Imam, I. El-Tantawy El-Sayed, M.G. Mahfouz, A.A. Tolba, T. Akashi, A.A. Galhoum, E. Guibal, Synthesis of α-aminophosphonate functionalized chitosan sorbents: Effect of methyl vs phenyl group on uranium sorption, Chem. Eng. J., 352 (2018) 1022-1034.
[29] A.M. Donia, A.A. Atia, K.Z. Elwakeel, Recovery of gold(III) and silver(I) on a chemically modified chitosan with magnetic properties, Hydrometallurgy, 87 (2007) 197-206.
[30] M.F. Hamza, A.A.H. Abdel-Rahman, S. Ramadan, H. Raslan, S. Wang, T. Vincent, E. Guibal, Functionalization of magnetic chitosan particles for the sorption of U(VI), Cu(II) and Zn(II)—Hydrazide derivative of glycine-grafted chitosan, Materials, 10 (2017) 539-560.
[31] R. Massart, Preparation of aqueous magnetic liquids in alkaline and acidic media, IEEE Trans. Magn., 17 (1981) 1247-1249.
[32] M.F. Hamza, A.A.H. Abdel-Rahman, E. Guibal, Magnetic glutamine-grafted polymer for the sorption of U(VI), Nd(III) and Dy(III), J. Chem. Technol. Biotechnol., 93 (2018) 1790-1806.
[33] M.F. Hamza, M.G. Mahfouz, A.A.H. Abdel-Rahman, Adsorption of uranium (VI) ions on hydrazinyl amine and 1,3,4-thiadiazol-2(3 H)-thion chelating resins, J. Dispersion Sci. Technol., 33 (2012) 1544-1551.
[34] M.V. Lopez-Ramon, F. Stoeckli, C. Moreno-Castilla, F. Carrasco-Marin, On the characterization of acidic and basic surface sites on carbons by various techniques, Carbon, 37 (1999) 1215-1221.
[35] W.J. Weber, J.C. Morris, Kinetics of adsorption on carbon from solutions., J. Sanitary Eng.Div. ASCE, 89 (1963) 31-60.
[36] S. Lagergren, About the theory of so-called adsorption of soluble substances., Kungliga Svenska Vetenskapsakademiens, 24 (1898) 1-39.
[37] Y.S. Ho, G. McKay, Pseudo-second order model for sorption processes, Proc. Biochem., 34 (1999) 451-465.
[38] I. Langmuir, The adsorption of gases on plane surfaces of glass, mica and platinum, J. Amer. Chem. Soc., 40 (1918) 1361-1402.
[39] K.Y. Foo, B.H. Hameed, Insights into the modeling of adsorption isotherm systems, Chem. Eng. J., 156 (2010) 2-10.
[40] H.M.F. Freundlich, Uber die adsorption in lasungen, Z. Phys. Chem., 57 (1906) 385-470.
[41] C. Tien, Adsorption Calculations and Modeling, Butterworth-Heinemann, Newton, MA, 1994,243 pp.
[42] WHO, Guidelines for drinking-water quality, 4th Ed. ed., World Health Organization, Geneva (Switzerland), 2011,541 pp.
[43] A.K. Galwey, M.E. Brown, Thermal Decomposition of Ionic Solids - Chemical Properties and Reactivities of Ionic Crystalline Phases, 1st ed., Elsevier, Amsterdam, The Netherlands, 1999,596 pp.
[44] G.Z. Kyzas, P.I. Siafaka, E.G. Pavlidou, K.J. Chrissafis, D.N. Bikiaris, Synthesis and adsorption application of succinyl-grafted chitosan for the simultaneous removal of zinc and cationic dye from binary hazardous mixtures, Chem. Eng. J., 259 (2015) 438-448.
[45] N.A.M. Zahri, S. Jamil, L.C. Abdullah, T.C.S. Yaw, M.N. Mobarekeh, S.J. Huey, N.S.M. Rapeia, Improved method for preparation of amidoxime modified poly(acrylonitrile-co-acrylic acid): Characterizations and adsorption case study, Polymers, 7 (2015) 1205-1220.

[46] S.S. Basarir, N.P. Bayramgil, The uranium recovery from aqueous solutions using amidoxime modified cellulose derivatives. III. Modification of hydroxypropylmethylcellulose with amidoxime groups, Cellulose, 20 (2013) 1511-1522.
[47] H.H. Abdel-Razik, E.R. Kenawy, Synthesis, characterization, and amidoximation of diaminomaleodinitrile-functionalized polyethylene terephthalate grafts for collecting heavy metals from wastewater, J. Appl. Polym. Sci., 125 (2012) 1136-1145.
[48] R. Williams, pKa data (compiled by R. Williams), http://www.chem.wisc.edu/areas/reich/pkatable/pKa_compilation-1-Williams.pdf, Accessed: 4/6/2017.
[49] I.F. Amaral, P.L. Granja, M.A. Barbosa, Chemical modification of chitosan by phosphorylation: an XPS, FT-IR and SEM study, J. Biomater. Sci., Polym. Ed., 16 (2005) 1575-1593.
[50] E. Desimoni, B. Brunetti, X-ray photoelectron spectroscopic characterization of chemically modified electrodes used as chemical sensors and biosensors: A review, Chemosensors, 3 (2015) 70-117.
[51] H. Maachou, M.J. Genet, D. Aliouche, C.C. Dupont-Gillain, P.G. Rouxhet, XPS analysis of chitosan-hydroxyapatite biomaterials: from elements to compounds, Surf. Interface Anal., 45 (2013) 1088-1097.
[52] W.F. Yap, W.M.M. Yunus, Z.A. Talib, N.A. Yusof, X-ray photoelectron spectroscopy and atomic force microscopy studies on crosslinked chitosan thin film., Int. J. Phys. Sci., 6 (International Journal of the Physical Sciences Vol. 6(11), pp. 2744-2749) 2744-2749.
[53] G. Beamson, D. Briggs, High Resolution XPS of Organic Polymers: The Scienta ESCA300 Database, Wiley, New York, NY, USA, 1992pp.
[54] A. Corrias, G. Mountjoy, D. Loche, V. Puntes, A. Falqui, M. Zanella, W.J. Parak, M.F. Casula, Identifying spinel phases in nearly monodisperse iron oxide colloidal nanocrystal, J. Phys. Chem. C, 113 (2009) 18667-18675.
[55] C.-H. Ho, C.-P. Tsai, C.-C. Chung, C.-Y. Tsai, F.-R. Chen, H.-J. Lin, C.-H. Lai, Shape-controlled growth and shape-dependent cation site occupancy of monodisperse Fe_3O_4 nanoparticles, Chem. Mater., 23 (2011) 1753-1760.
[56] F. Kraushofer, Z. Jakub, M. Bichler, J. Hulva, P. Drmota, M. Weinold, M. Schmid, M. Setvin, U. Diebold, P. Blaha, G.S. Parkinson, Atomic-scale structure of the hematite alpha-Fe_2O_3(1(1)over-bar02) "R-Cut" Surface, J. Phys. Chem. C, 122 (2018) 1657-1669.
[57] D. Wilson, M.A. Langell, XPS analysis of oleylamine/oleic acid capped Fe_3O_4 nanoparticles as a function of temperature, Appl. Surf. Sci., 303 (2014) 6-13.
[58] B. Lindberg, R. Maripuu, K. Siegbahn, R. Larsson, C.G. Golander, J.C. Eriksson, ESCA studies of heparinized and related surfaces. 1. Model surfaces on steel substrates., J. Colloid Interface Sci., 95 (1983) 308-321.
[59] R.S. Vieira, M.L.M. Oliveira, E. Guibal, E. Rodriguez-Castellon, M.M. Beppu, Copper, mercury and chromium adsorption on natural and crosslinked chitosan films: An XPS investigation of mechanism, Colloids Surf., A, 374 (2011) 108-114.
[60] S.A. Chambers, S.A. Joyce, Surface termination, composition and reconstruction of Fe_3O_4(001) and gamma-Fe_2O_3(001), Surf. Sci., 420 (1999) 111-122.
[61] T. Droubay, S.A. Chambers, Surface-sensitive Fe 2p photoemission spectra for alpha-Fe_2O_3(0001): The influence of symmetry and crystal-field strength, Physical Review B, 64 (2001).
[62] L. Minati, V. Micheli, B. Rossi, C. Migliaresi, L. Dalbosco, G. Bao, S. Hou, G. Speranza, Application of factor analysis to XPS valence band of superparamagnetic iron oxide nanoparticles, Appl. Surf. Sci., 257 (2011) 10863-10868.

[63] N.B. Dewage, R.E. Fowler, C.U. Pittman, Jr., D. Mohan, T. Mlsna, Lead (Pb^{2+}) sorptive removal using chitosan-modified biochar: batch and fixed-bed studies, RSC Adv., 8 (2018) 25368-25377.
[64] J.-P. Simonin, On the comparison of pseudo-first order and pseudo-second order rate laws in the modeling of adsorption kinetics, Chem. Eng. J., 300 (2016) 254-263.
[65] I. Persson, Hydrated metal ions in aqueous solution: How regular are their structures?, Pure Appl. Chem., 82 (2010) 1901-1917.
[66] Y. Marcus, Ion Properties, Marcel Dekker, Inc., New York, NY, 1997,259 pp.
[67] Y.J. Yang, S.D. Alexandratos, Affinity of polymer-supported reagents for lanthanides as a function of donor atom polarizability, Ind. Eng. Chem. Res., 48 (2009) 6173-6187.
[68] R.G. Pearson, Acids and bases, Science, 151 (1966) 172-177.
[69] J.D. Giraldo, B.L. Rivas, E. Elgueta, A. Mancisidor, Metal ion sorption by chitosan-tripolyphosphate beads, J. Appl. Polym. Sci., 134 (2017).
[70] Z. Yang, X. Huang, X. Yao, H. Ji, Thiourea modified hyper-crosslinked polystyrene resin for heavy metal ions removal from aqueous solutions, J. Appl. Polym. Sci., 135 (2018).
[71] C. Xiong, C. Yao, Ion exchange recovery of nickel(II) on macroporous weak acid resin (D151 resin), Indian J. Chem. Technol., 18 (2011) 13-20.
[72] T. Hajeeth, K. Vijayalakshmi, T. Gomathi, P.N. Sudha, Removal of Cu(II) and Ni(II) using cellulose extracted from sisal fiber and cellulose-g-acrylic acid copolymer, Int. J. Biol. Macromol., 62 (2013) 59-65.
[73] S.D. Alexandratos, X. Zhu, The effect of hydrogen bonding in enhancing the ionic affinities of immobilized monoprotic phosphate ligands, Materials, 10 (2017).
[74] P. Michard, E. Guibal, T. Vincent, P. LeCloirec, Sorption and desorption of uranyl ions by silica gel: pH, particle size and porosity effects, Microporous Mater., 5 (1996) 309-324.
[75] V.C. Srivastava, I.D. Mall, I.M. Mishra, Equilibrium modelling of single and binary adsorption of cadmium and nickel onto bagasse fly ash, Chem. Eng. J., 117 (2006) 79-91.
[76] S.R. Popuri, Y. Vijaya, V.M. Boddu, K. Abburi, Adsorptive removal of copper and nickel ions from water using chitosan coated PVC beads, Bioresour. Technol., 100 (2009) 194-199.
[77] E. Uguzdogan, E.B. Denkbas, O.S. Kabasakal, The use of polyethyleneglycolmethacrylate-co-vinylimidazole (PEGMA-co-VI) microspheres for the removal of nickel(II) and chromium(VI) ions, J. Hazard. Mater., 177 (2010) 119-125.
[78] M. Monier, D.M. Ayad, Y. Wei, A.A. Sarhan, Preparation and characterization of magnetic chelating resin based on chitosan for adsorption of Cu(II), Co(II), and Ni(II) ions, React. Funct. Polym., 70 (2010) 257-266.
[79] N. Dizge, B. Keskinler, H. Barlas, Sorption of Ni(II) ions from aqueous solution by Lewatit cation-exchange resin, J. Hazard. Mater., 167 (2009) 915-926.
[80] A.F. Shaaban, A.A. Khalil, M. Radwan, M. El Hefnawy, H.A. El Khawaga, Synthesis, characterization and application of a novel nanometer-sized chelating resin for removal of Cu(II), Co(II) and Ni(II) ions from aqueous solutions, J Polym Res, 24 (2017) 165-178.
[81] X. Song, H. Du, S. Liu, H. Qian, Adsorption properties of Ni(II) by D301R anion exchange resin, J. Chem., 2014 (2014) Art. ID 407146.
[82] B.A. Fil, R. Boncukcuoglu, A.E. Yilmaz, S. Bayar, Adsorption of Ni(II) on ion exchange resin: Kinetics, equilibrium and thermodynamic studies, Korean J. Chem. Eng., 29 (2012) 1232-1238.
[83] R.R. Bhatt, B.A. Shah, Sorption studies of heavy metal ions by salicylic acid-formaldehyde-catechol terpolymeric resin: Isotherm, kinetic and thermodynamics, Arabian J. Chem., 8 (2015) 414-426.

[84] M. Ceglowski, G. Schroeder, Preparation of porous resin with Schiff base chelating groups for removal of heavy metal ions from aqueous solutions, Chem. Eng. J., 263 (2015) 402-411.
[85] T.E. Khalil, A. El-Dissouky, S. Rizk, Equilibrium and kinetic studies on Pb^{2+}, Cd^{2+}, Cu^{2+} and Ni^{2+} adsorption from aqueous solution by resin 2, 2'- (ethylenedithio)diethanol immobilized Amberlite XAD-16 (EDTDE-AXAD-16) with chlorosulphonic acid, J. Mol. Liq., 219 (2016) 533-546.
[86] V. Gomez-Serrano, A. Macias-Garcia, A. Espinosa-Mansilla, C. Valenzuela-Calahorro, Adsorption of mercury, cadmium and lead from aqueous solution on heat-treated and sulphurized activated carbon, Water Res., 32 (1998) 1-4.
[87] G. Bayramoglu, I. Tuzun, G. Celik, M. Yilmaz, M.Y. Arica, Biosorption of mercury(II), cadmium(II) and lead(II) ions from aqueous system by microalgae *Chlamydomonas reinhardtii* immobilized in alginate beads, Int. J. Miner. Process., 81 (2006) 35-43.
[88] D. Mohan, H. Kumar, A. Sarswat, M. Alexandre-Franco, C.U. Pittman, Jr., Cadmium and lead remediation using magnetic oak wood and oak bark fast pyrolysis bio-chars, Chem. Eng. J., 236 (2014) 513-528.
[89] S.A. Ahmed, Removal of lead and sodium ions from aqueous media using natural wastes for desalination and water purification, Desalin. Water Treat, 57 (2016) 8911-8926.
[90] S. Deniz, N. Tasci, E.K. Yetimoglu, M.V. Kahraman, New thiamine functionalized silica microparticles as a sorbent for the removal of lead, mercury and cadmium ions from aqueous media, J. Serb. Chem. Soc., 82 (2017) 215-226.
[91] L. Tofan, C. Paduraru, I. Cretescu, A. Ceica, V. Neagu, Chelating sorbent containing two types of functional groups - hydroxamic acid and amidoxime for lead(II) ions effluent management, Environ. Eng. Manage. J., 9 (2010) 113-118.
[92] M.K. Othman, F.A. Al-Qadri, F.A. Al-Yusufy, Synthesis, physical studies and uptake behavior of: copper(II) and lead(II) by Schiff base chelating resins, Spectrochim. Acta, Part A, 78 (2011) 1342-1348.
[93] S.A. Abo-Farha, A.Y. Abdel-Aal, I.A. Ashour, S.E. Garamon, Removal of some heavy metal cations by synthetic resin purolite C100, J. Hazard. Mater., 169 (2009) 190-194.
[94] O. Arar, Removal of lead(II) from water by di (2-ethylhexyl) phosphate containing ion exchange resin, Desalin. Water Treat, 52 (2014) 3197-3205.
[95] F. Hayeeye, Q.J. Yu, M. Sattar, W. Chinpa, O. Sirichote, Adsorption of Pb^{2+} ions from aqueous solutions by gelatin/activated carbon composite bead form, Adsorpt. Sci. Technol., 36 (2018) 355-371.
[96] L. Zhang, Y. Wang, J. Huang, S. Yuan, Azido chelating fiber: synthesis, characterization and adsorption performances towards Hg^{2+} and Pb^{2+} from water, Polym. Adv. Technol., 28 (2017) 1418-1427.

Table 1: Uptake kinetics for Ni(II) and Pb(II) binding on HA-MG-CH sorbent – Parameters of the models.

Model	Parameter	Ni(II)	Pb(II)
Experimental	$q_{eq,exp}$	3.88	2.19
PFORE	$q_{eq,1}$	3.88	2.20
	$k_1 \times 10^2$	8.91	36.2
	EV	0.027	0.008
	R^2	0.978	0.984
PSORE	$q_{eq,2}$	4.12	2.35
	$k_2 \times 10^2$	3.71	24.2
	EV	0.052	0.020
	R^2	0.973	0.962

Table 2: Sorption isotherms for Ni(II) and Pb(II) binding on HA-MG-CH sorbent – Parameters of the models.

Model	Parameter	Ni(II)	Pb(II)
Experimental	$q_{m,exp}$	3.90	2.63
Langmuir	$q_{m,L}$	4.33	2.51
	b_L	2.64	35.2
	EV	0.025	0.095
	R^2	0.989	0.922
Freundlich	k_F	2.67	2.47
	n_F	3.12	4.26
	EV	0.247	0.046
	R^2	0.901	0.955
Sips	$q_{m,S}$	4.26	4.94
	b_S	2.88	1.02
	n_S	0.956	2.90
	EV	0.030	0.048
	R^2	0.990	0.961

Table 3: Comparison of sorption properties for conventional sorbents and biosorbents

Metal	Sorbent	pH	t_{eq} (min)	q_m (mmol g^{-1})	b (L $mmol^{-1}$)	Reference
Ni(II)	Bagasse fly ash	6.0	120	0.111	9.01	[75]
	Chitosan-coated PVC beads	5.0	240	2.05	2.05	[76]
	Synthetic polymer microspheres	7.0	120	0.77	-	[77]
	Cellulose	5.0	360	4.88	1.19	[72]
	Cellulose-g-acrylic acid	5.0	360	5.10	0.57	[72]
	Magnetic Schiff's base derivative of chitosan resin	5.0	120	0.80	1.35	[78]
	Lewatit MonoPlus SP 112 resin	6.0	90	2.91	95.1	[79]
	Nanometer-sized chelating resin	6.4	180	1.182	0.542	[80]
	D301R ion exchange resin	8.0	120	1.31	2.00	[81]
	D151 (macro- weak acid resin)	6.9	1440	5.16	322.9	[71]
	Dowex HCR-S cationic resin	6.0	60	1.60	3.02	[82]
	Salicylic acid /formaldehyde /catechol resin	6.0	240	0.815	3.06	[83]
	Schiff base chelating resin	5.0	300	1.15	0.763	[84]
	Modified Amberlite XAD-16 resin	-	60	0.764	24.5	[85]
	HA-MG-CH	5.0	60	4.33	2.64	*This work*
Pb(II)	Sulphurized activated carbon	5.4	-	≈ 0.3	-	[86]
	Chlamydomonas reinhardtii / alginate beads	6.0	90	1.84	20.56	[87]
	Magnetic oak bark biochar	5.0	60	0.146	194.8	[88]
	Sugarcane bagasse	5.0	60	0.0054	64.1	[89]
	Beet pulp	5.0	60	00090	0.058	[89]
	Mercaptoamine functionalized silica-coated magnetic nanosorbent	6-7	120	1.41	4.14	[12]
	Thiamine-functionalized silica microparticles	5.0	120	0.19	-	[90]
	Hydroxamic acid/amidoxime bifunctional acrylic acid resin	-	-	0.94	-	[91]
	Schiff base chelating resin	10	120	0.50	0.50	[92]
	Purolite C100 resin	5-6	1440	0.046	3.31	[93]
	Modified Amberlite XAD-16 resin	-	60	0.519	2409	[85]
	Di (2-ethylhexyl) phosphate containing ion exchange resin	4	80	0.172	94.7	[94]
	Gelatin/activated carbon beads	5	60	1.79	1.14	[95]
	Thiourea-modified hyper-crosslinked polystyrene resin	6.0		3.33	7.0	[70]
	Salicylic acid /formaldehyde /catechol resin	6.0	240	0.931	16.1	[83]
	Chitosan-tripolyphosphate	5.0	1080	1.21	41.4	[69]
	Azido chelating fiber	6.0	1440	1.50	32.9	[96]
	HA-MG-CH	5.0	60	2.51	35.2	*This work*

-: Missing information.

Table 4: Sorption/desorption performances (sorption capacity at equilibrium (q_{eq} (mmol g^{-1}) and desorption efficiency (DE, %)) for the recovery of Ni(II) and Pb(II) using HA-MG-CH sorbent.

Metal	Ni(II)				Pb(II)			
Run #	q_{eq}		DE (%)		q_{eq}		DE (%)	
	Aver.	SD (%)	Aver.	SD (%)	Aver.	SD (%)	Aver.	SD (%)
1	214.9	2.0	98.3	1.5	513.1	0.9	99.3	0.8
2	209.0	2.6	99.8	0.8	510.0	0.5	96.0	0.7
3	203.5	1.4	101.0	2.2	502.7	0.4	98.5	2.3
4	197.8	0.1	97.7	0.6	492.7	0.6	96.0	0.4
5	197.3	1.1	95.3	2.6	489.9	1.0	97.7	2.3
Aver. DE(%)	-	-	98.4	2.0	-	-	97.5	1.3
Max. Loss in q_{eq} (%)	8.2				4.5			

Aver.: average value; SD (%): standard deviation (%).

Table 5: Sorption performance from multi-metal equimolar concentration for two contact times (C_0: ≈ 0.2 mmol metal L^{-1}; pH_0: 5.01; pH(30 min): 4.78; pH(60 min): 4.05; SD: 2.5 g L^{-1}).

	t: 30 min					t: 60 min			
Metal	C_0 (a)	C_{30} (a)	q_{30} (b)	K_d (c)	Eff. (%)	C_{60} (a)	q_{60} (b)	K_d (c)	Eff. (%)
Al(III)	5.3	4.02	0.119	0.80	24.2	3.28	0.187	1.54	38.1
Cd(II)	21.2	9.98	0.225	2.81	52.9	1.93	0.429	25.0	90.9
Cu(II)	12.7	4.91	0.306	3.97	61.3	0.89	0.465	33.2	93.0
Ni(II)	11.3	5.32	0.255	2.81	52.9	1.09	0.435	23.4	90.4
Pb(II)	44.2	11.9	0.390	6.79	73.1	1.74	0.512	61.0	96.1
Cr(VI)	11.8	8.44	0.162	1.00	28.5	4.94	0.330	3.47	58.1
Total	≈ 1.22[d]		0.481			0.274[d]	2.358		77.4

a: mg L^{-1}; b: mmol g^{-1}; c: L g^{-1}; d: mmol L^{-1}.

Table 6: Stormwater treatment – Effect of contact time on residual metal concentrations (sorbent dosage: 250 mg L^{-1}).

			Contact time						At 5h		
Metal	C_0 (µmol L^{-1})	C_0 (mg L^{-1})	30 min	1 h	2 h	3 h	4 h	5 h	Eff. (%)	K_d (L g^{-1})	MCL
Al(III)	229.4	6.19	5.79	4.22	0.94	0.3	**0.12**	**0.1**	98.4	244	0.2
Cd(II)	0.623	0.07	0.07	0.06	0.01	0.009	0.005	**0.003**	95.7	89.3	0.003
Cu(II)	52.1	3.35	2.08	**1.06**	**0.65**	**0.15**	**0.09**	**0.07**	97.9	187	2
Ni(II)	15.7	0.92	0.9	0.39	0.09	**0.05**	**0.05**	**0.05**	94.6	69.6	0.07
Pb(II)	31.5	6.53	3.11	1.98	0.25	0.06	0.05	0.02	99.7	1302	0.01
Cr(VI)	1.54	0.08	0.08	0.06	**0.04**	**0.04**	**0.04**	**0.04**	50.0	4	0.05
pH		6.33	6.21	6.01	5.65	5.17	5.15	5.06	-	-	-

Bold: residual concentrations conform to MCL for drinking water standards (WHO)

Table 7: Stormwater treatment – Effect of contact time on residual metal concentrations and final recovery efficient (at 5 h of contact) (sorbent dosage: 500 mg L^{-1}).

			Contact time						At 5h		
Metal	C_0 (µmol L^{-1})	C_0 (mg L^{-1})	30 min	1 h	2 h	3 h	4 h	5 h	Eff. (%)	K_d (L g^{-1})	MCL
Al(III)	229.4	6.19	3.82	1.99	**0.02**	**0.02**	**0.02**	**0.02**	99.7	617	0.2
Cd(II)	0.623	0.07	0.05	0.02	**0.003**	**0.003**	**0.003**	**0.003**	95.7	44.7	0.003
Cu(II)	52.1	3.35	**1.76**	**0.89**	**0.11**	**0.09**	**0.09**	**0.09**	97.3	72.4	2
Ni(II)	15.7	0.92	0.63	0.21	**0.06**	**0.05**	**0.05**	**0.05**	94.6	34.8	0.07
Pb(II)	31.5	6.53	2.32	0.71	**0.009**	**0.009**	**0.009**	**0.009**	99.9	1449	0.01
Cr(VI)	1.54	0.08	0.06	**0.05**	**0.04**	**0.04**	**0.04**	**0.04**	50.0	2	0.05
pH		6.33	6.01	5.87	5.25	4.94	4.93	4.93	-	-	-

Bold: residual concentrations conform to MCL for drinking water standards (WHO)

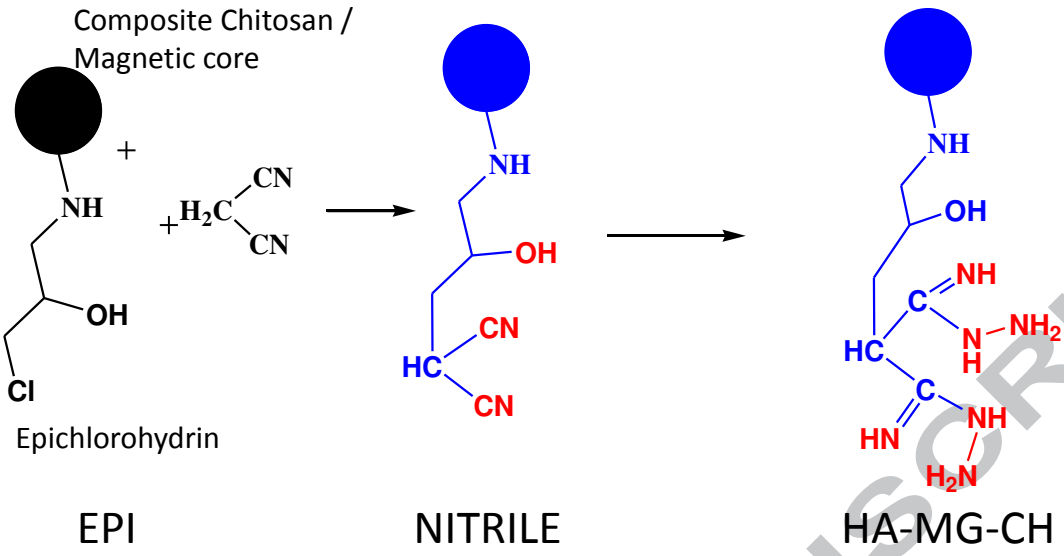

Figure 1: Schematic representation of HA-MG-CH synthesis and structure.

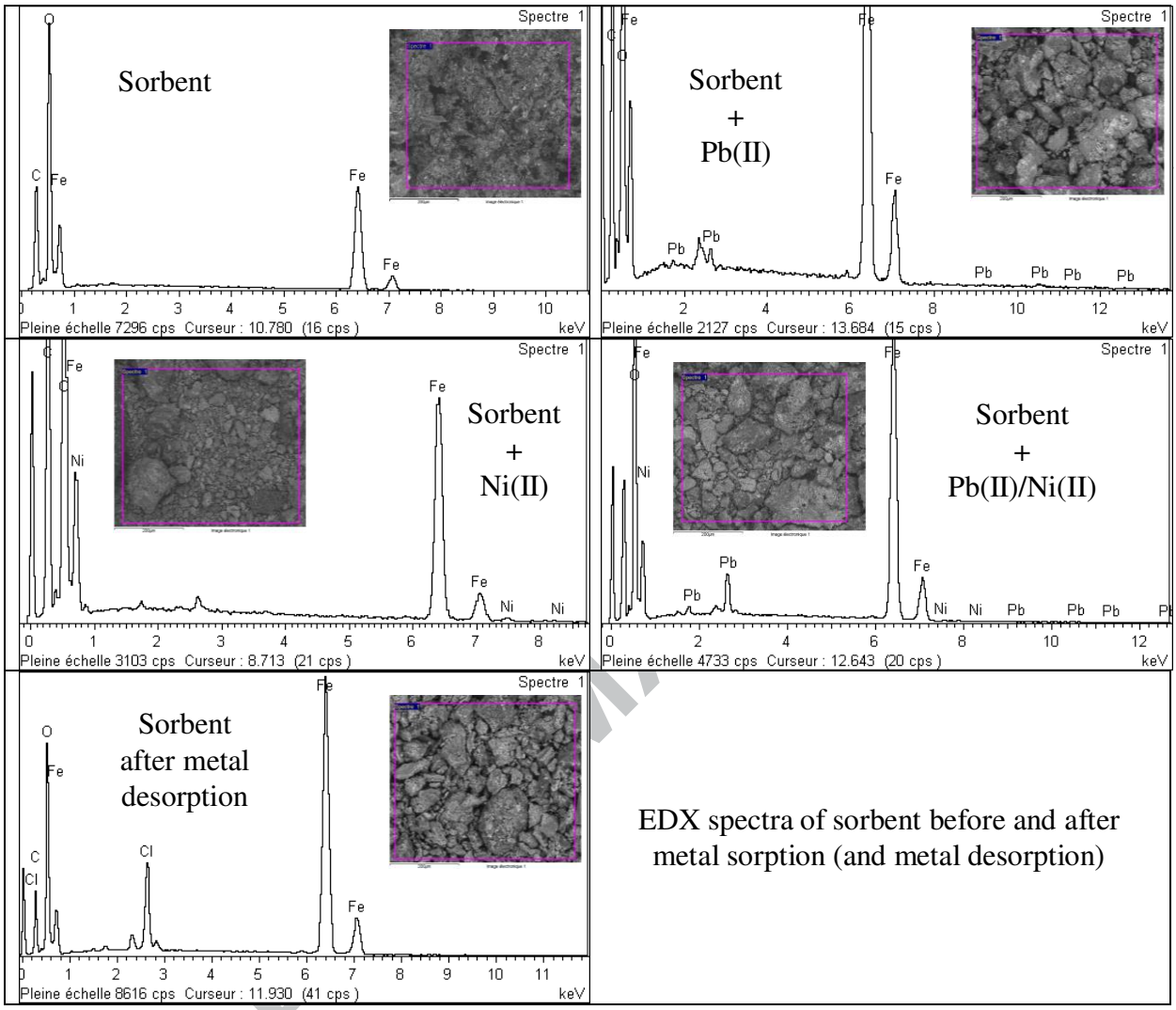

Figure 2: Sorbent characterization before and after Pb(II), Ni(II) and Pb(II)/Ni(II) sorption and after metal desorption (SEM micrograph and EDX spectra).

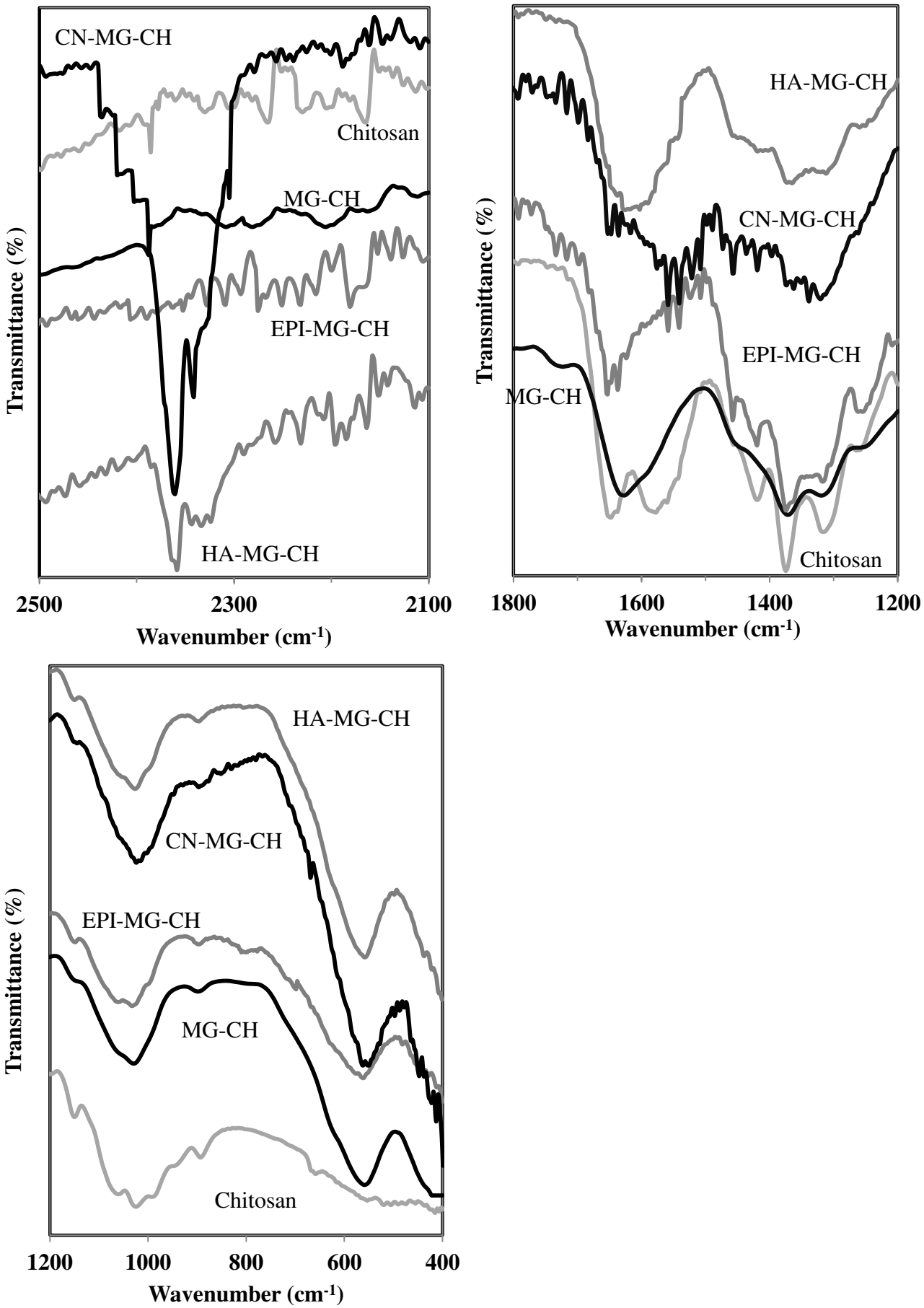

Figure 3: FTIR spectra of chitosan, MG-CH, EPI-MG-CH, CN-MG-CH and HA-MG-CH.

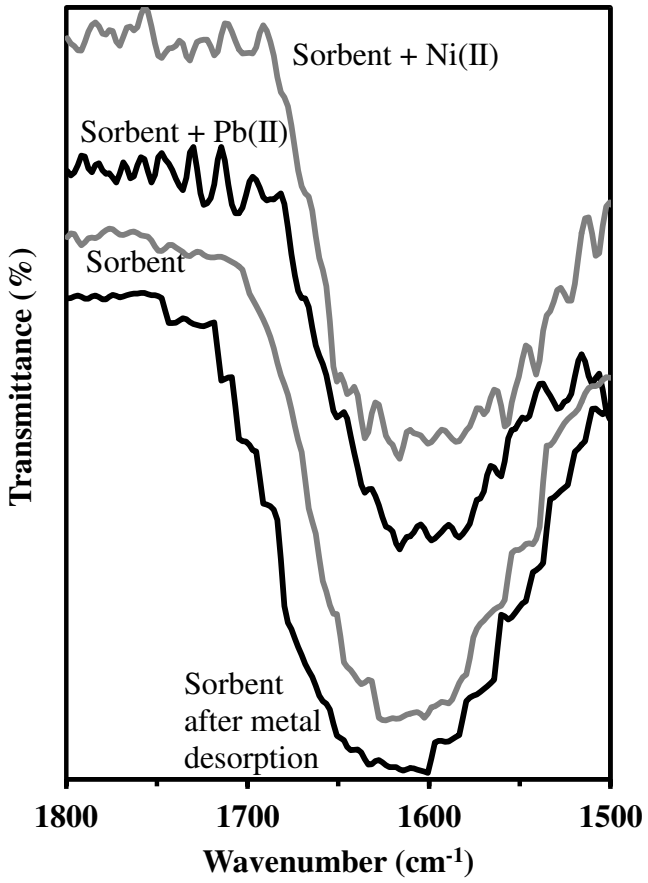

Figure 4: FTIR spectra of sorbent before and after Pb(II), and Ni(II) sorption and after metal desorption.

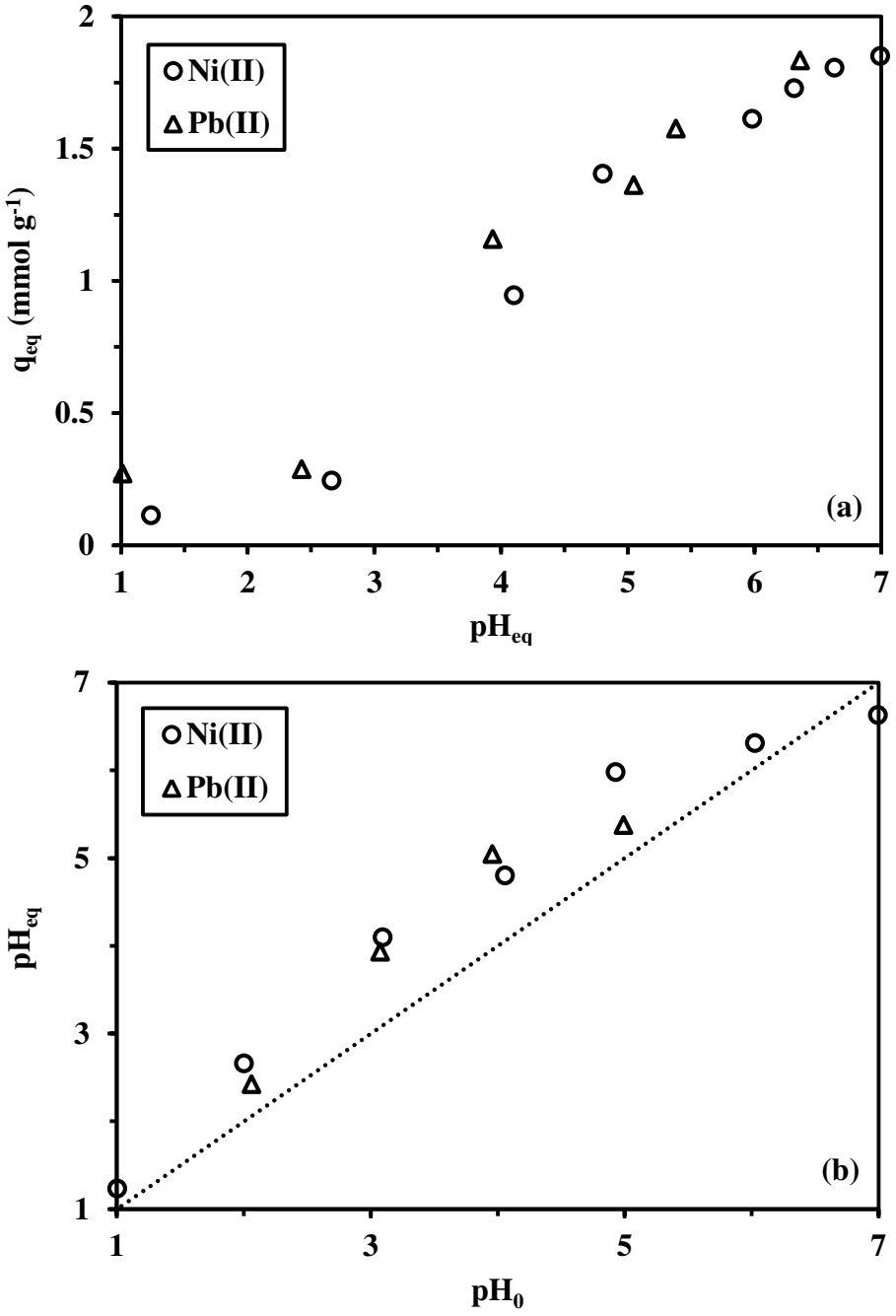

Figure 5: Effect of pH on Ni(II) and Pb(II) sorption using HA-MG-CH sorbent: (a) effect on sorption capacity, (b) pH variation during metal sorption (Sorbent dosage, SD: 166 mg L^{-1}; C_0: 0.635 mmol Ni L^{-1} and 0.364 mmol Pb L^{-1}; T: 25 °C; contact time: 48 h).

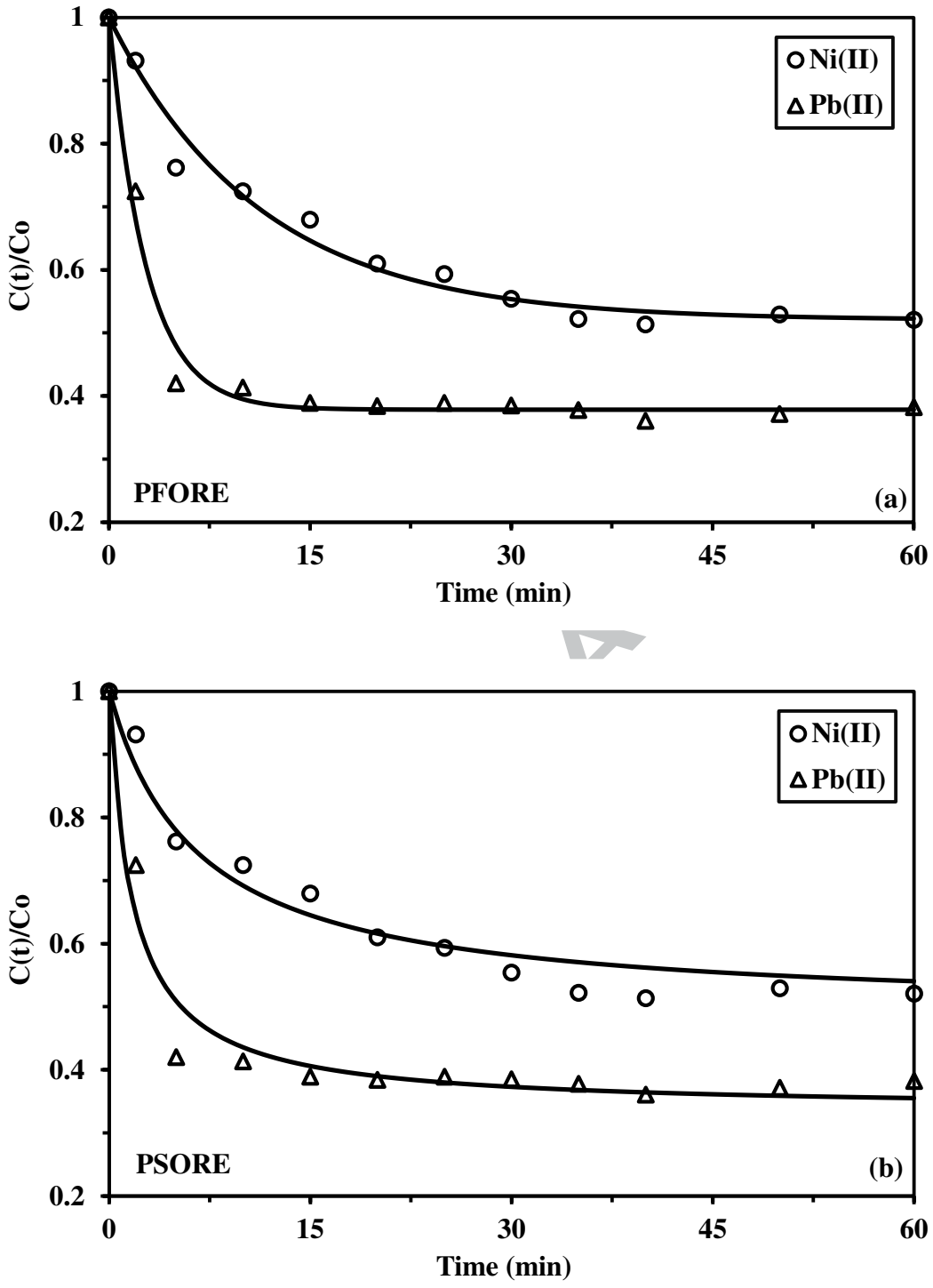

Figure 6: Uptake kinetics for Ni(II) and Pb(II) sorption on HA-MG-CH sorbent: (a) PFORE fit, (b) PSORE fit (for Ni(II): SD: 250 mg L^{-1}; C_0: 2.02 mmol Ni L^{-1}; pH_0: 5.07; pH_{eq}: 6.00 - for Pb(II): SD: 200 mg L^{-1}; C_0: 0.708 mmol Pb L^{-1}; pH_0: 5.08; pH_{eq}: 5.88; T: 25 °C).

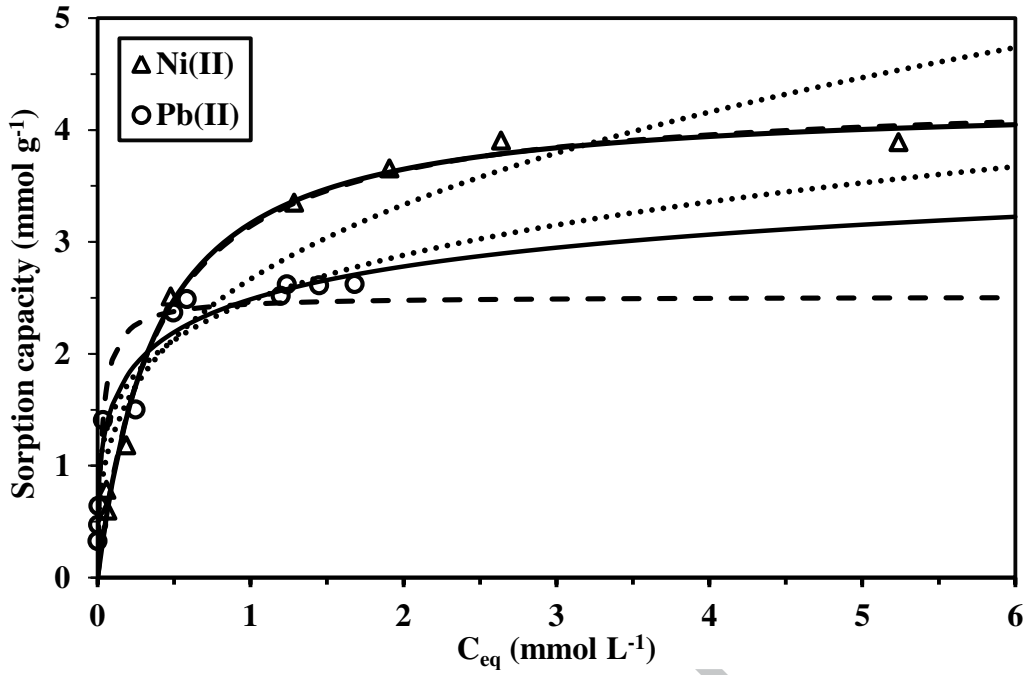

Figure 7: Sorption isotherms for Ni(II) and Pb(II) sorption on HA-MG-CH sorbent – Modeling with Langmuir equation (- -), Freundlich equation (····) and Sips equation (—) (for Ni(II): SD: 170 mg L^{-1}; C_0: 0.13-5.94 mmol Ni L^{-1}; pH_0: 5.0-5.1; pH_{eq}: 5.3-6.8 - for Pb(II): SD: 140 mg L^{-1}; C_0: 0.02-2.54 mmol Pb L^{-1}; pH_0: 5-5.1; pH_{eq}: 4.8-6.9; T: 25 °C).

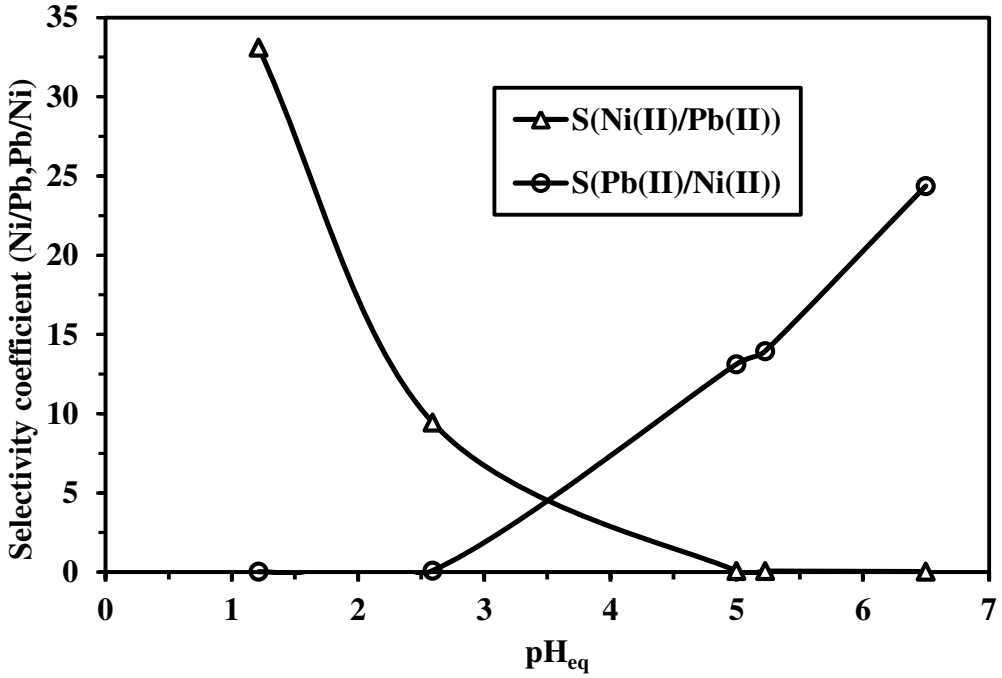

Figure 8: Metal sorption from bi-component solutions –Evolution of selectivity coefficients SC(Ni(II)/Pb(II)) and SC(Pb(II)/Ni(II)) as a function of equilibrium pH (C_0: 0.65 mmol L^{-1}, equimolar in Ni(II) and Pb(II); SD: 400 mg L^{-1}; T: 25 °C; contact time: 48 h).

Highlights

- Efficient grafting of hydrazinyl amine on chitosan-coated magnetite.
- High sorption capacity for divalent metals at near neutral pH.
- Sorption isotherms are fitted by Sips equation.
- Sorbent can be reused for at least 5 cycles using 0.5 M HCl as eluent.
- Selectivity for Pb(II) for decontaminating multi-metal stormwater.